

C IV absorption in damped and sub-damped Lyman- α systems

Correlations with metallicity and implications for galactic winds at $z \approx 2 - 3^*$

Andrew J. Fox¹, Cédric Ledoux², Patrick Petitjean^{1,3}, & Raghunathan Srianand⁴

¹ Institut d'Astrophysique de Paris, UMR7095 CNRS, Université Pierre et Marie Curie, 98bis Blvd Arago, 75014 Paris, France

² European Southern Observatory, Alonso de Córdova 3107, Casilla 19001, Vitacura, Santiago 19, Chile

³ LERMA, Observatoire de Paris, 61 Avenue de l'Observatoire, 75014 Paris, France

⁴ IUCAA, Post Bag 4, Ganesh Khind, Pune 411 007, India

Received April 13, 2007 / Accepted July 27, 2007

ABSTRACT

We present a study of C IV absorption in a sample of 63 damped Lyman- α (DLA) systems and 11 sub-DLAs in the redshift range $1.75 < z_{\text{abs}} < 3.61$, using a dataset of high-resolution (6.6 km s^{-1} FWHM), high signal-to-noise VLT/UVES spectra. Narrow and broad C IV absorption line components indicate the presence of both warm, photoionized and hot, collisionally ionized gas. We report new correlations between the metallicity (measured in the neutral-phase) and each of the C IV column density, the C IV total line width, and the maximum C IV velocity. We explore the effect on these correlations of the sub-DLAs, the proximate DLAs (defined as those within 5000 km s^{-1} of the quasar), the saturated absorbers, and the metal line used to measure the metallicity, and we find the correlations to be robust. There is no evidence for any difference between the measured properties of DLA C IV and sub-DLA C IV. In 25 DLAs and 4 sub-DLAs, covering 2.5 dex in $[Z/H]$, we directly observe C IV moving above the escape speed, where v_{esc} is derived from the total line width of the neutral gas profiles. These high-velocity C IV clouds, unbound from the central potential well, can be interpreted as highly ionized outflowing winds, which are predicted by numerical simulations of galaxy feedback. The distribution of C IV column density in DLAs and sub-DLAs is similar to the distribution in Lyman Break galaxies, where winds are directly observed, supporting the idea that supernova feedback creates the ionized gas in DLAs. The unbound C IV absorbers show a median mass flow rate of $\sim 22 (r/40 \text{ kpc}) M_{\odot} \text{ yr}^{-1}$, where r is the characteristic C IV radius. Their kinetic energy fluxes are large enough that a star formation rate (SFR) of $\sim 2 M_{\odot} \text{ yr}^{-1}$ is required to power them.

Key words. quasars: absorption lines – cosmology: observations – galaxies: high-redshift – galaxies: halos – galaxies: ISM

1. Introduction

To study the properties of high-redshift galaxies in a luminosity-independent manner, one can analyze the absorption lines imprinted by their gaseous halos on the spectra of background quasars. Such halos are thought to give rise to QSO absorption line system of various H I column densities: the damped Lyman- α systems (DLAs), with $\log N_{\text{H I}} > 20.3$, the sub-DLAs with $19.0 < \log N_{\text{H I}} < 20.3$, and the Lyman limit systems (LLSs) with $17.0 < \log N_{\text{H I}} < 19.0$. Observations have shown that highly ionized gas, as detected in O VI and C IV absorption, is present in each of these categories of absorber at $z \gtrsim 2$: in DLAs (Lu et al. 1996; Ledoux et al. 1998; Wolfe & Prochaska 2000a; Fox et al. 2007), in sub-DLAs, (Dessauges-Zavadsky et al. 2003; Péroux et al. 2003; Richter et al. 2005), and in LLSs (Bergeron et al. 1994; Kirkman & Tytler 1997, 1999). As one progresses down in H I column density from DLAs to LLSs, one may be sampling progressively more remote (and more highly

ionized) regions of Galactic halos, with most gas in LLSs lying outside the halo virial radius (Maller et al. 2003; Davé et al. 1999). Even some O VI absorbers associated with Lyman- α forest clouds, which are thought to represent the low-density intergalactic medium (IGM), may arise in extended galaxy halos or feedback zones from galactic outflows (Bergeron & Herbert-Fort 2005; Simcoe et al. 2006).

Studying this protogalactic plasma allows one to address two key themes of extragalactic astronomy: galactic winds and the metal budget. Galactic winds are common at high redshift (Veilleux et al. 2005), and must be present in order to enrich the IGM up to its observed metallicity (Aguirre et al. 2001, 2005; Aracil et al. 2004). Simulations predict that the level of ionization in winds is high (Oppenheimer & Davé 2006; Kawata & Rauch 2007; Fangano et al. 2007), and direct observations of absorption in high-ionization lines have been made in and around Lyman Break galaxies (LBGs; Pettini et al. 2000, 2002; Shapley et al. 2003; Adelberger et al. 2005). Low-redshift studies of galactic outflows have also found a high-ionization component (Heckman et al. 2001; Strickland et al. 2004). Since DLAs represent the largest reservoirs of neutral gas for high-redshift star formation

* Based on observations taken with the Ultraviolet and Visual Echelle Spectrograph (UVES) on the Very Large Telescope (VLT) Unit 2 (Kueyen) at Paranal, Chile, operated by ESO.

(Wolfe et al. 2005), they are natural sites to look for supernova-driven winds and plasma halos in general.

On the second front, ionized halos are important because of their potential ability to close the metal budget at $z \approx 2$: there is currently a discrepancy between the global density of metals predicted by integrating the star formation history, and the density of metals actually observed (Pettini 1999; Ferrara et al. 2005; Bouché et al. 2005, 2006, 2007; Sommer-Larsen & Fynbo 2007). The contribution of plasma halos to the metal budget will be particularly significant if the plasma is hot and collisionally ionized, because the cooling times in low-metallicity, low-density, hot halos are extremely long, and so gas injected into these environments can become locked up until the current epoch. For 10^6 K gas at 10^{-3} cm^{-3} and solar metallicity, t_{cool} is 2.4×10^8 yr (Houck & Bregman 1990), so assuming that to first order $t_{\text{cool}} \propto Z^{-1}$, we find that the cooling time in gas at one-hundredth solar metallicity (as seen in DLAs) would be approximately equal to the Hubble time. Finding the gas in hot halos is therefore important for tracing the history of the cosmic metals.

In a recent paper (Fox et al. 2007, hereafter Paper I), we discussed the first observations of O VI absorption in DLAs, finding evidence for a hot ionized medium that, modulo certain assumptions on metallicity and ionization, typically contains $\gtrsim 40\%$ as many baryons and metals as there are in the neutral phase. Though 12 DLAs with O VI detections were found, detailed kinematic measurements of the O VI absorption are difficult due to the high density of blends with the Lyman- α forest. However, if one instead traces the ionized gas with C IV, whose lines lie redward of the Lyman- α forest, the blending problems are avoided. Thus, although C IV may trace a lower temperature phase of plasma than O VI, it is a better ion to study for building a sample of statistical size. Partly for this reason, the properties of C IV absorption in the IGM at $z > 2$ have been studied at length (Cowie & Songaila 1998; Ellison et al. 2000; Schaye et al. 2003; Boksenberg et al. 2003; Aracil et al. 2004; Aguirre et al. 2005; Songaila 2005, 2006; Scannapieco et al. 2006a; Schaye et al. 2007).

Previous observations of C IV absorption in DLAs (Lu et al. 1996; Ledoux et al. 1998; Wolfe & Prochaska 2000a) and sub-DLAs (Dessauges-Zavadsky et al. 2003; Péroux et al. 2003; Richter et al. 2005; Péroux et al. 2007) have found the C IV profiles generally occupy a more extended (though overlapping) velocity range than the neutral gas profiles. In an attempt to explain these observations, Wolfe & Prochaska (2000b) tested a model of gas falling radially onto centrifugally-supported exponential disks, and found it was unable to reproduce the observed C IV kinematics. On the other hand, Maller et al. (2003) found that a model in which hot gas in halos and sub-halos gives rise to the C IV absorption in DLAs was generally successful in explaining the kinematics.

We continue the study of C IV in DLAs in this paper. We are partly motivated by the recent work of Ledoux et al. (2006), who reported a correlation between low-ion line width Δv_{Neut} and metallicity $[Z/H]$ in a sample of 70 DLAs and sub-DLAs, covering over two orders of magnitude in metallicity (see also Wolfe & Prochaska 1998; Murphy et al. 2007; Prochaska et al. 2007a). Since the line widths of the neutral species are thought to be gravitationally-dominated, the broader lines may be tracing the more massive halos, and so the $\Delta v_{\text{Neut}}-[Z/H]$ correlation

has been interpreted as evidence for an underlying mass-metallicity relation. A natural follow-on question is whether a similar correlation exists between the *high-ion* line width and DLA metallicity. In this paper we investigate whether such a correlation exists, as well as exploring other relations between the properties of C IV and those of the neutral gas. To maximize our sample size, we include observations of C IV absorption in both DLAs and sub-DLAs (and we compare the properties of the C IV absorption in the two samples). There is some evidence that sub-DLAs display larger metallicities than DLAs (Dessauges-Zavadsky et al. 2003; Péroux et al. 2005; Kulkarni et al. 2007), and they have been suggested to be more massive (Khare et al. 2007).

The structure of this paper is as follows. Sect. 2 covers the observations, sample selection, and measurements. In Sect. 3 we present observed correlations in the data set. In Sect. 4 we discuss the interpretation of these correlations, and we identify a population of absorbers that may trace galactic winds. A summary is presented in Sect. 5.

2. Data acquisition and handling

2.1. Observations

Our dataset was formed by combining the DLA/sub-DLA sample of Ledoux et al. (2006) with the Hamburg-ESO DLA survey of Smette et al. (2005, 2007, in preparation). All the data were taken in the years 2000 to 2006 with the Very Large Telescope/Ultraviolet-Visual Echelle Spectrograph (VLT/UVES), located on the 8.2 m VLT Unit 2 telescope (Kueyen) at Cerro Paranal, Chile. UVES is described in Dekker et al. (2000). The data reduction was performed as described in Ledoux et al. (2003), using the interactive pipeline written by Ballester et al. (2000), running on the ESO data reduction system MIDAS. The rebinned pixel size is $\approx 2 \text{ km s}^{-1}$ and the data have a spectral resolution (FWHM) of 6.6 km s^{-1} ($R=45\,000$).

2.2. C IV sample selection

We took the 81 DLAs and sub-DLAs in the raw sample with data covering C IV, and looked for C IV components in a range of $\pm 1000 \text{ km s}^{-1}$ around the system redshift. Absorption line components were identified as C IV if they were present in both $\lambda 1548$ and $\lambda 1550$ in the correct (2:1) doublet ratio. In four cases the C IV lines were so contaminated by blends that we rejected them from the sample. In three other cases, the H I lines or neutral-phase metal lines were too blended for a metallicity to be derived; these were also excluded. No DLAs or sub-DLAs were found where C IV absorption is not present. The final sample contains 63 DLAs and 11 sub-DLAs, which are listed in Table 1. Five of the DLAs and two sub-DLA are at less than 5000 km s^{-1} from the QSO redshift, and so may be affected by radiation from the QSO (e.g. Ellison et al. 2002). For completeness we retain these $z_{\text{abs}} \approx z_{\text{qso}}$ systems (also known as proximate systems) in the sample, but the corresponding data points are highlighted in all figures, and we take note of any differences from the intervening population.

2.3. Measurement

2.3.1. Apparent Column Density

For each DLA and sub-DLA, we fit a continuum to a region several thousand km s^{-1} in width centered on C IV $\lambda 1548$, using a polynomial fit (often linear) to regions of the spectrum judged to be free from absorption. We defined the zero-point of the velocity scale using the redshift of the strongest component of neutral gas absorption. We then determined v_- and v_+ , the velocities where the C IV absorption recovers to the continuum on the blueward and redward side of the line. For each pixel between v_- and v_+ , the apparent optical depth is defined as $\tau_a(v) = \ln[F_c(v)/F(v)]$, where $F(v)$ and $F_c(v)$ are the actual flux and the estimated continuum flux as a function of velocity, respectively. The total apparent optical depth is then found by integrating over the line, i.e. $\tau_a = \int_{v_-}^{v_+} \tau_a(v) dv$. The apparent column density in each absorber then follows by $N_a = [3.768 \times 10^{14} / (\lambda_0 f)] \tau_a$ (Savage & Sembach 1991), where λ_0 is in Angstroms, and f is the oscillator strength of the line. For the two C IV lines, we take $\lambda_0 = 1548.204, 1550.781 \text{ \AA}$ and $f = 0.1899, 0.09475$ from Morton (2003); see also Petitjean & Aracil (2004). The apparent column density will equal the true column density so long as the lines are not heavily saturated, and that there is no unresolved saturation in the line profiles.

2.3.2. Total Line Width

We require a precise measurement of the total C IV line width in each system. Following Prochaska & Wolfe (1997), we define $\Delta v_{\text{C IV}}$ as the velocity width that contains the central 90% of the integrated optical depth in the line. By finding the two pixels where the cumulative integrated optical depth is 5% and 95% of the total, and determining the velocity difference between them, one obtains $\Delta v_{\text{C IV}}$. This can be done for each of the two lines in the C IV doublet, with the same result expected in each case if the lines are unsaturated and unblended. Note that $\Delta v_{\text{C IV}}$ is integrated over all components, and should not be confused with the line widths of each individual component.

We also define an alternative measure of total line width as $v_+ - v_-$, the total velocity range over which C IV absorption is present, regardless of saturation. $v_+ - v_-$ is sensitive to weak but nonetheless interesting satellite components that are not contained within $\Delta v_{\text{C IV}}$. These weak components are particularly relevant in the search for winds. The drawback of using $v_+ - v_-$ is that it has a larger error than $\Delta v_{\text{C IV}}$, since v_- and v_+ are selected by eye (we estimate $\sigma_{v_+ - v_-} = 20 \text{ km s}^{-1}$), and also that it is sensitive to the signal-to-noise ratio (low optical depth absorption is harder to detect in low S/N data). Our data is of high enough quality to ensure that the second effect should not be a major concern: the noisiest spectrum in our sample has $S/N=25$, and the mean S/N is 51 (where the S/N is measured per resolution element at the observed wavelength of C IV).

2.3.3. Mean and Maximum C IV Velocity

For each profile, we measure the average optical depth-weighted velocity, denoted by $\bar{v}_{\text{C IV}}$, and calculated by $\bar{v}_{\text{C IV}} = \int_{v_-}^{v_+} v \tau_a(v) dv / \int_{v_-}^{v_+} \tau_a(v) dv$. Since the velocity zero-point is defined by the strongest absorption component in

the neutral gas, $\bar{v}_{\text{C IV}}$ is equivalent to the mean velocity offset between the neutral and ionized gas. In the analysis we are only concerned with the magnitude of the velocity offset, $|\bar{v}|$, and not whether the gas is blueshifted or redshifted relative to the neutral gas. We also make use of v_{max} , the maximum absolute velocity at which C IV absorption is observed (i.e., the terminal velocity), given by $v_{\text{max}} = \max(|v_-|, |v_+|)$.

2.3.4. Choice of Doublet Line

The measurements of column density, total line width, and mean velocity were conducted independently on $\lambda 1548$ and $\lambda 1550$. To select which of the two C IV transitions to use for our final measurement, we followed the following rules that assess the influence of saturation. If the condition $F(v_0)/F_c(v_0) > 0.1$ (corresponding to $\tau_a(v_0) < 2.3$) is true for $\lambda 1548$, where v_0 denotes the velocity where the absorption is strongest, we use $\lambda 1548$ to measure the C IV, otherwise we use $\lambda 1550$. If both lines are saturated (defined here as when $F(v) < \sigma_{F(v)}$ or $F(v) < 0.03 F_c(v)$ at any point within the line profile), we proceed with a lower limit to the column density and an upper limit to the line width using the results from $\lambda 1550$. However, if one of the two C IV lines is blended, we use the other line for measurement, regardless of the level of saturation. There are four cases where both C IV lines are partly blended, but we still have useful information at other velocities within the line profiles. This can occur when the two C IV lines, separated by $\approx 500 \text{ km s}^{-1}$, blend with each other. In these cases, which are flagged in Table 1, we derived our best estimate of $\log N_{\text{C IV}}$ using the sum of the column densities measured over two separate unblended velocity ranges, and assuming $\Delta v_{\text{C IV}} = 0.9(v_+ - v_-)$ and $\bar{v} = (v_- + v_+)/2$, where for these cases v_- refers to the lower bound of absorption of the lower velocity range, and v_+ refers to the upper bound of absorption of the higher velocity range.

2.3.5. Properties of the Neutral Phase

In most of the systems in our sample, the metallicity of the neutral gas, the H I column density, and the low-ion line width have already been published in Ledoux et al. (2006), so we take these measurements directly from that paper. We also include measurements of $[\text{Zn}/\text{H}]$ in two DLAs (at $z_{\text{abs}} = 2.34736$ toward Q0438-0436 and 2.18210 toward Q2311-373) from Akerman et al. (2005), one DLA and one sub-DLA (at $z_{\text{abs}} = 1.85733$ and 1.87519, respectively, toward Q2314-409) from Ellison & Lopez (2001), and two DLAs (at $z_{\text{abs}} = 2.40186$ toward Q0027-186 and 1.98888 toward Q2318-111) from Noterdaeme et al. (2007). For the remaining cases where no neutral-phase measurements have been published, we executed the measurements using exactly the same techniques as in Ledoux et al. (2006). The metal line used to measure $[\text{Z}/\text{H}]$ is Zn II if detected, otherwise Si II or S II, and $N_{\text{H I}}$ is derived from a fit to the damping wings of the Lyman- α line. Both zinc and silicon are found to be undepleted in DLAs (Prochaska & Wolfe 2002), so these metallicities should not be significantly affected by dust. We follow the standard practise of quoting metallicities on a logarithmic scale relative to solar. All measurements were adjusted to the solar reference levels adopted by Morton (2003).

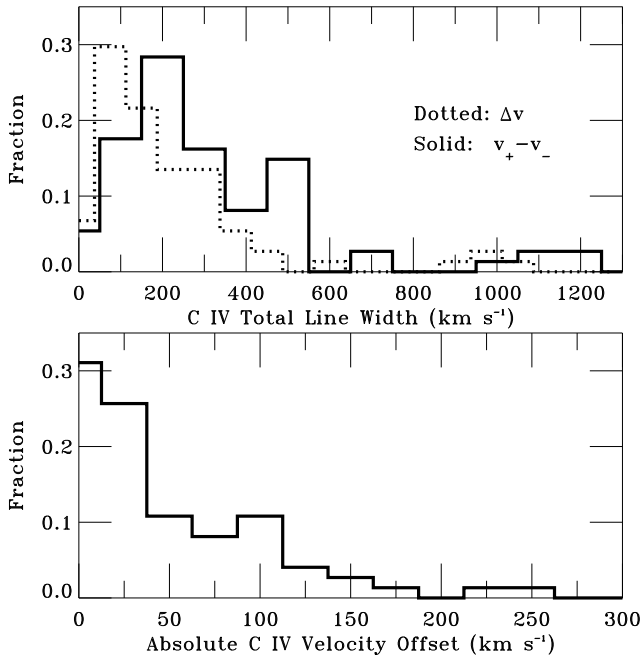


Fig. 2. Normalized histograms of total C IV line width and absolute velocity offset among our DLA/sub-DLA sample. The distribution of both Δv (dotted) and $v_+ - v_-$ (solid) is shown in the top panel. The peak of the $v_+ - v_-$ distribution is $\approx 100 \text{ km s}^{-1}$ broader than the peak of the Δv distribution, reflecting the presence of low optical depth satellite components. There is an extended tail of line widths reaching $> 1000 \text{ km s}^{-1}$. We have treated the upper limits to Δv as data points when forming the distribution. The distribution of the absolute C IV velocity offset (i.e., the mean C IV velocity relative to the neutral gas) is shown in the lower panel.

3. Results

The measurements of C IV absorption in each of the 74 systems are given in Table 1, and the C IV profiles for each system (together with an optically thin line showing the component structure in the neutral phase) are shown in Fig. 1. Our sample spans a redshift range from 1.75 to 3.61 with a median of 2.34. The values of $\log N_{\text{H I}}$ range from 19.70 to 21.80 with a median of 20.65, and the metallicity $[Z/H]$ lies between -2.59 and -0.31 with a median of -1.36 (i.e., approximately one twentieth of the solar value). The values of $\log N_{\text{C IV}}$ range from 13.02 to > 15.41 (median value 14.15), with total line widths $\Delta v_{\text{C IV}}$ between 35 and 1110 km s^{-1} (median value 187 km s^{-1}), and velocity offsets between 0 and 425 km s^{-1} (median value 46 km s^{-1}).

Histograms of the total C IV line width (using both Δv and $v_+ - v_-$) and C IV velocity offset are given in Fig. 2. A significant difference between the distributions of Δv and $v_+ - v_-$ can be seen, with the peak in the Δv distribution at $\approx 80 \text{ km s}^{-1}$, and the peak in the $v_+ - v_-$ distribution occurring at $\approx 200 \text{ km s}^{-1}$. This difference is due to the presence of weak, outlying components which contribute to $v_+ - v_-$ but not to Δv . Both distributions show an extended tail reaching over 1000 km s^{-1} . Fig. 2 also shows the distribution of mean C IV velocities.

3.1. DLA C IV vs IGM C IV

C IV absorbers in the IGM falling at velocities within 1000 km s^{-1} of the DLA/sub-DLA would not necessarily be physically connected to the system. Such IGM C IV would contaminate our sample, in particular by contributing to the high $\Delta v_{\text{C IV}}$ tail shown in the top panel of Fig. 2. IGM contamination could be occurring in systems where outlying, discrete components are seen at velocities separated from the bulk of the absorption by hundreds of km s^{-1} (e.g., $z_{\text{abs}} = 2.293$ toward Q0216+080, $z_{\text{abs}} = 2.347$ toward Q0438-436, $z_{\text{abs}} = 1.825$ toward Q1242+001, and $z_{\text{abs}} = 2.154$ toward Q2359-022). However, we do not wish to exclude these absorbers from our sample, since then we would be biased against finding high-velocity features, such as winds. Our approach is thus to systematically include all C IV absorption in a fixed velocity interval around the system.

We can assess the level of IGM contamination statistically by comparing the properties of the C IV in our sample with those of C IV in the IGM. This is shown in Fig. 3, where we compare our DLA/sub-DLA C IV column density distribution with the IGM distribution at $z \approx 2-3$ measured by Boksenberg et al. (2003, data taken from their Fig. 10). A similar IGM C IV distribution is presented by Songaila (2005). We also include in Fig. 3 the distribution of C IV near LBGs, taken from Table 3 in Adelberger et al. (2005); these measurements were made by finding LBGs lying at impact parameters of $< 1 h_{70}^{-1}$ co-moving Mpc from QSO sight lines, and then measuring the C IV column densities in the QSO spectra at velocities within 200 km s^{-1} of the LBG redshift. Strong C IV absorption is also directly observed in LBG spectra by Shapley et al. (2003).

The DLA/sub-DLA C IV absorbers are clearly a different population from the IGM C IV absorbers: the DLA/sub-DLA population shows a mean column density that is higher by almost 1 dex. The distribution of C IV in DLAs and sub-DLAs resembles the distribution of galactic C IV as seen in LBGs, both with mean column densities near 10^{14} cm^{-2} . In consequence, the highest $N_{\text{C IV}}$ systems in our sample are *least* likely to be of IGM origin. Since we report below that the highest $N_{\text{C IV}}$ systems tend to show the broadest C IV, we come to the conclusion that even the broadest C IV absorbers (that were potentially the most suspect in terms of an association with an individual galaxy), are likely to be galactic.

We now discuss correlations (or lack thereof) between the various measured quantities in our dataset. For reference, a summary of all correlations found and their statistical significance is given in Table 2.

3.2. High-ion line width vs low-ion line width

In Fig. 4 we directly compare the high-ion total line width with the low-ion total line width for each DLA and sub-DLA in the sample. In almost all cases (69 of 74) the C IV lines cover a wider region of velocity space than the neutral lines; this finding has been reported by Ledoux et al. (1998) and Wolfe & Prochaska (2000a). We also find a considerable scatter (≈ 1 dex) in $\Delta v_{\text{C IV}}$ at low Δv_{Neut} , but the scatter decreases with increasing Δv_{Neut} .

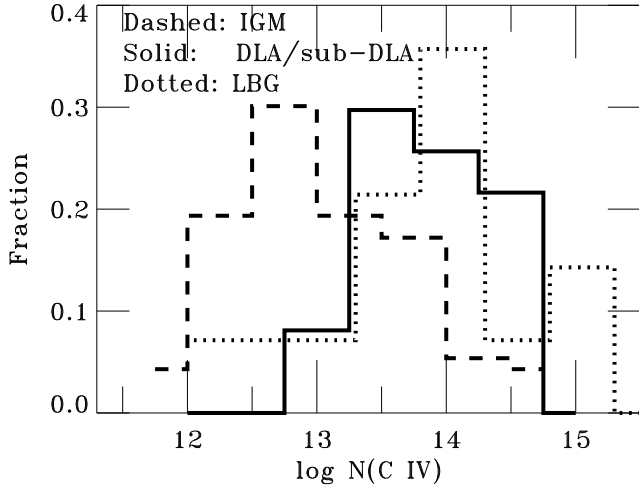


Fig. 3. Comparison of the normalized C IV column density distributions: (i) in DLAs and sub-DLAs (solid line, this work); (ii) in the IGM at $z \approx 2 - 3$ (dashed line; Boksenberg et al. 2003); (iii) around LBGs at $z \approx 2 - 3$ (dotted line; Adelberger et al. 2005). In each case, $N_{\text{C IV}}$ is integrated over all components. Note how a typical DLA/sub-DLA shows (a) considerably stronger C IV than a typical IGM C IV absorber, but (b) a C IV column similar to the mean seen in the LBG distribution. These two findings support our interpretation that the C IV in DLAs and sub-DLAs is galactic rather than intergalactic. We have included the saturated C IV absorbers as data points in the DLA/sub-DLA distribution, using the measured lower limits; this has the effect of artificially truncating the high $N_{\text{C IV}}$ tail of the solid line.

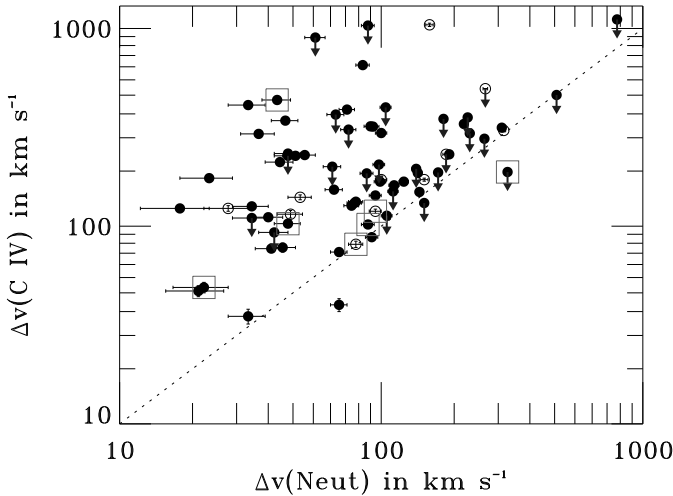


Fig. 4. Comparison of high-ion and low-ion total line width for DLAs (filled circles) and sub-DLAs (open circles). Absorbers at $< 5000 \text{ km s}^{-1}$ from the QSO redshift are highlighted in square symbols. The dashed line shows where $\Delta v_{\text{C IV}} = \Delta v_{\text{Neut}}$. In 69 of 74 cases the C IV absorption is broader than the neutral absorption. There is a large scatter in $\Delta v_{\text{C IV}}$ at low Δv_{Neut} , but the scatter decreases with increasing Δv_{Neut} . Saturated C IV absorbers are shown with upper limits to $\Delta v_{\text{C IV}}$.

3.3. Internal correlations of C IV properties

We find that the C IV column density, total line width, and velocity offset are all correlated with one another. This is shown in Fig. 5, which illustrates a $> 6.0\sigma$ correlation between $N_{\text{C IV}}$ and $(v_+ - v_-)_{\text{C IV}}$, and a 4.3σ correlation between $\bar{v}_{\text{C IV}}$ and $(v_+ - v_-)_{\text{C IV}}$. We investigated whether these two correlations were still found when removing the proximate absorbers and the sub-DLAs from the sample, and found that they were, at $> 6.0\sigma$ and 3.8σ significance, respectively (see Table 2). Finally, we considered the effect of the lower limits on the $N_{\text{C IV}}$ vs $(v_+ - v_-)_{\text{C IV}}$ correlation, by redoing the analysis with the saturated points excluded. We still found a correlation, but the slope (in log-log space) is lower by ~ 0.6 dex in this case (see Fig. 5). In summary, the DLAs and sub-DLAs with strong C IV absorption tend to show broader and more offset C IV profiles.

3.4. Metallicity vs C IV column density

We plot $N_{\text{C IV}}$ vs $[Z/H]$ in Fig. 6. panel (a). We emphasize that the metallicity is not derived from the C IV lines, but is measured independently in the neutral phase of absorption, using either the Zn II/H I, Si II/H I, or S II/H I ratio. A Kendall rank correlation test shows that the two quantities are correlated at $> 6.0\sigma$ significance (where the limits were included in the analysis). Almost all the high-metallicity DLAs show saturated C IV lines, which are shown with arrows to represent lower limits to $N_{\text{C IV}}$. The correlation is still found (at 5.1σ) when only using the intervening DLAs, and is also detected (at 3.5σ) when only using the cases with $[Z/H]$ derived from Zn II (since these metallicities are more robust against dust depletion effects). Finally the correlation is still found (but only at 2.5σ) when only considering the unsaturated C IV data points (i.e., when ignoring the lower limits). The detection of this correlation confirms the tentative result found in Paper I based on a much smaller sample of twelve DLAs.

A linear least-squares bisector fit to the data gives the result:

$$\begin{aligned} \log N_{\text{C IV}} &= (1.2 \pm 0.1)[Z/H] + (15.8 \pm 0.2) \quad [\text{all points}] \quad (1) \\ \log N_{\text{C IV}} &= (1.0 \pm 0.1)[Z/H] + (15.4 \pm 0.2) \quad [\text{no limits}], \end{aligned}$$

where $N_{\text{C IV}}$ is expressed in cm^{-2} , the errors in the slope and y-intercept represent the 1σ uncertainties, and the first and second equations describe the cases where the limits are included and excluded in the fit, respectively.

3.5. Metallicity vs C IV total line width

In Fig. 6 panel (b) we find evidence for a loose correlation between metallicity and $\Delta v_{\text{C IV}}$. A Kendall τ test shows a 3.4σ correlation when using all 74 DLAs and sub-DLAs. If we restrict the sample to the 58 DLAs at $> 5000 \text{ km s}^{-1}$ from the QSO, to remove the effects of sub-DLAs and proximity to the quasar, the significance of the correlation decreases to 2.9σ . Working just with the DLAs and sub-DLAs with metallicities derived from Zn II, the significance is 2.6σ .

If we remove the upper limits on $\Delta v_{\text{C IV}}$ (i.e., the saturated absorbers) from the sample, and redo the correlation analysis, we find no significant detection of a correlation between $[Z/H]$ and $\Delta v_{\text{C IV}}$ remains. However, in a sense this is not surprising, since the saturated absorbers tend to show

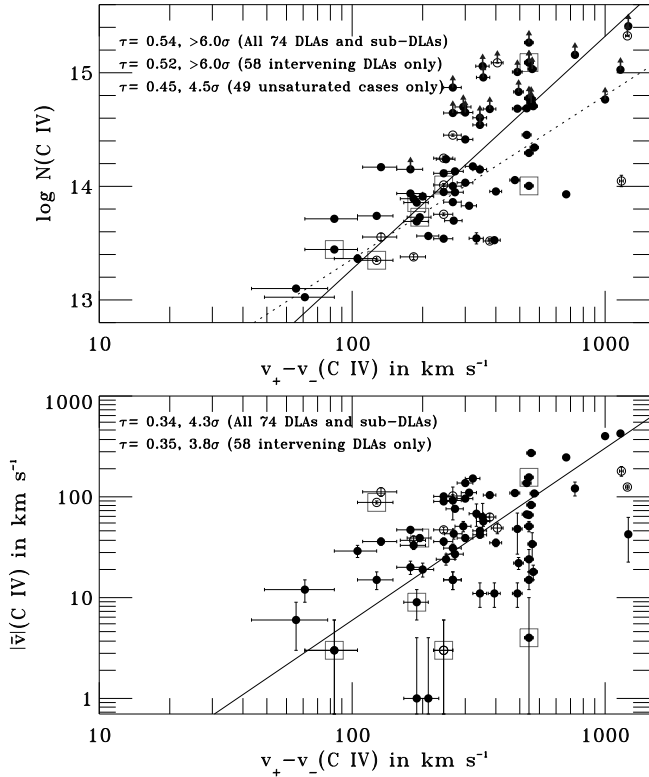


Fig. 5. Correlations between the measured C IV properties for both DLAs (filled circles) and sub-DLAs (open circles). Proximate absorbers are highlighted in square symbols. We use $v_+ - v_-$ rather than Δv to measure the line width, since it is defined even in the saturated cases. We annotate the Kendall rank correlation coefficient τ and its significance on the panel, for various sub-samples. Solid lines show linear least-square bisector fits for the case where all data points are treated equally (including limits). **Top panel:** C IV column density vs C IV line width. A correlation is found even when excluding the saturated C IV absorbers (the lower limits on $N_{\text{C IV}}$), although in this case the slope of the fit (shown as a dashed line) is shallower. **Bottom panel:** comparison between total C IV line width and C IV absolute velocity offset, also showing a significant correlation. These trends show that the stronger C IV absorbers tend to be broader and more offset from the neutral gas than the weaker absorbers.

broad C IV lines (Sect. 3.4), so by removing them, we are biased against finding a trend with line width. To further investigate whether saturation was playing a role in setting up this metallicity-line width relation, we looked for a correlation between $[Z/H]$ and $(v_+ - v_-)_{\text{C IV}}$. As discussed in Sect. 2.3.2, $(v_+ - v_-)_{\text{C IV}}$ is defined even in the saturated cases. The result was that we detected a positive correlation at the 4.1σ level. Since we believe this metallicity-C IV line width correlation to be one of the most important results of this paper, we investigated whether it was seen independently in the lower- and higher- redshift halves of the sample, and found that it was at $\approx 3\sigma$ significance (Fig. 7), even though the mean metallicity of the low-redshift sample is higher than the mean metallicity of the high-redshift sample. Together, these results imply that the C IV line width and metallicity are correlated in DLAs and sub-DLAs.

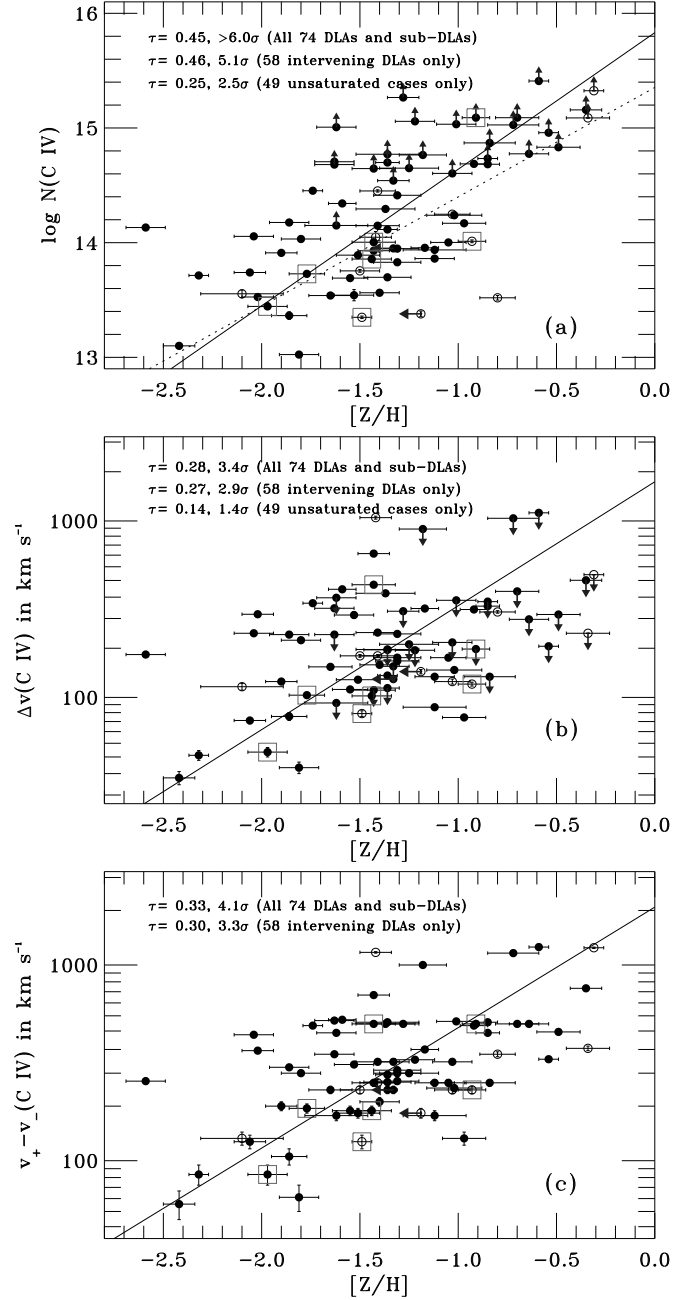


Fig. 6. Dependence of C IV properties in DLAs (filled circles) and sub-DLAs (open circles) with neutral-phase metallicity. Proximate absorbers are highlighted in square symbols. In each panel, we annotate the Kendall rank correlation coefficient τ and its significance, and we show a linear least-square bisector fit (solid line), for the case where all data points are treated equally (including the limits). In panel (a), we find a significant correlation between $N_{\text{C IV}}$ and $[Z/H]$. This remains true (at 2.5σ) even in the case where the saturated points are excluded, though in this case the slope is slightly shallower (dashed line). In panel (b), we show a 3.4σ correlation between $\Delta v_{\text{C IV}}$ and $[Z/H]$, but this correlation is *not* found when the saturated points are excluded (hence there is no dashed line in this panel). However, if we instead use $(v_+ - v_-)_{\text{C IV}}$ to measure the line width (bottom panel), since this statistic is not affected by saturation, a significant (4.1σ) metallicity-line width correlation does exist. The detected correlations show that high-metallicity systems tend to exhibit strong and broad C IV absorption.

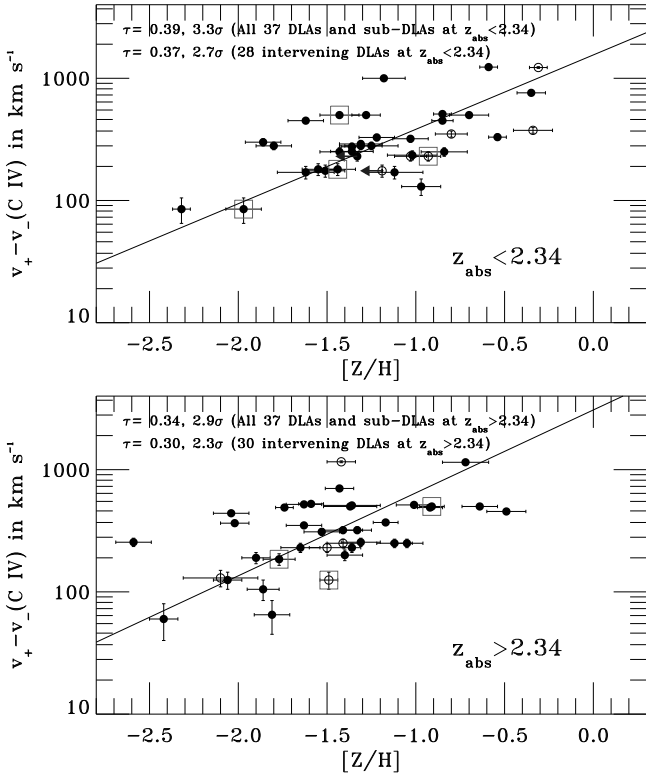


Fig. 7. Illustration that the correlation between C IV total line width and metallicity exists independently in the lower and upper redshift halves of the sample, even though there is a difference between the mean metallicity of the two sub-samples (the lower- z sample shows systematically higher $[Z/H]$). The symbols have their same meanings as in Fig. 6. All DLAs and sub-DLAs in each redshift range were included in the correlation analysis and in the linear bisector fits, shown with solid lines.

Using the sample of 74 DLAs and sub-DLAs, the best-fit linear least-squares bisector model is:

$$[Z/H] = (1.4 \pm 0.1) \log \Delta v_{C\,IV} - (4.6 \pm 0.5), \quad (2)$$

where again the errors are the 1σ uncertainties, and where $\Delta v_{C\,IV}$ is in km s^{-1} . The slope of this relation is similar to that found for the low-ion total line width/metallicity correlation by Ledoux et al. (2006), who report $[Z/H] = (1.55 \pm 0.12) \log \Delta v_{\text{Neut}} - (4.33 \pm 0.23)$. However, we observe a large dispersion in total C IV line width at a given metallicity, far larger than the measurement errors, and also larger than the dispersion seen in the low-ion line width/metallicity correlation.

There are four DLAs (at $z_{\text{abs}} = 2.418$ toward Q0112+306, $z_{\text{abs}} = 2.076$ toward Q2206-199, $z_{\text{abs}} = 2.153$ toward Q2222-396, and $z_{\text{abs}} = 2.537$ toward Q2344+125), and one sub-DLA (at $z_{\text{abs}} = 3.170$ toward Q1451+123) that stand out on Fig. 6(b) and 6(c). due to their unusual properties. These absorbers show narrow C IV lines ($\Delta v_{C\,IV} < 50 \text{ km s}^{-1}$ in all cases), low velocity offsets ($|\bar{v}|_{C\,IV} < 10 \text{ km s}^{-1}$ in four of five cases), and low metallicities ($[Z/H]$ between -2.42 and -1.81). These cases play a significant role in generating the correlations discussed here.

3.6. Metallicity vs C IV velocity offset and terminal velocity

Over our sample of 74 DLAs and sub-DLAs, the mean value of $|\bar{v}|_{C\,IV}$ is 69 km s^{-1} . $|\bar{v}|_{C\,IV}$ is not correlated with the metallicity. However, the absolute maximum C IV velocity v_{max} is correlated with the metallicity at the 2.9σ level (not shown in figures, but see Table 2). The significance of this correlation decreases to 2.6σ when just using the intervening DLA sample. Saturation has no effect on the maximum C IV velocity, so we included the saturated C IV absorbers in this correlation analysis. We note that v_{max} reaches over 200 km s^{-1} in 42 cases, and $>500 \text{ km s}^{-1}$ in 8 cases.

3.7. H I column density versus high ions

We find that none of the C IV properties (column density, total line width, and mean velocity) correlate with $N_{\text{H I}}$, even though our sample covers two orders of magnitude in $N_{\text{H I}}$. In Table 3 we compare the observed properties of C IV absorption in DLAs ($\log N_{\text{H I}} > 20.3$) with those in sub-DLAs ($\log N_{\text{H I}} < 20.3$). There is no significant difference between the two populations in mean column density, mean total line width, or mean velocity offset from the neutral gas. However, if we assume that the ionization fraction C IV/C is the same in all systems, then the DLAs tend to show larger H II column densities than the sub-DLAs (see Sect. 3.9).

3.8. Intervening vs proximate systems

The differences between proximate DLAs and intervening DLAs have been studied in recent years (Ellison et al. 2002; Russell et al. 2006; Hennawi & Prochaska 2007; Prochaska et al. 2007b). Here we compare the properties of the C IV absorption in proximate and intervening DLAs and sub-DLAs. These results are relevant to claims that photoevaporation by the quasar reduces the H I cross-section in proximate DLAs (Hennawi & Prochaska 2007; Prochaska et al. 2007b). We find no evidence for a higher degree of ionization in the proximate systems. Indeed, the mean C IV column densities and total line widths in the proximate systems are slightly *lower* than the corresponding values in the intervening systems. However, our current proximate sample with C IV only contains seven systems, so further data are needed before strong conclusions can be drawn.

3.9. Total ionized column density

One of the key conclusions of Paper I was that, if the ionized and neutral phases of DLA have the same metallicity, then the H II column density in the O VI phase typically amounts to $>40\%$ of the H I column density in the neutral phase, and that $N_{\text{H II}}$ in the C IV phase amounts to a further $>20\%$ of $N_{\text{H I}}$. These percentages are important since they determine the total quantity of baryons and metals hidden in the ionized gas. With the much larger sample in this paper, we are able to improve upon the second of these estimates. $N_{\text{H II}}$ in the C IV phase is calculated by:

$$N_{\text{H II}} = \frac{N_{C\,IV}}{f_{C\,IV} C/H} = \frac{N_{C\,IV}}{f_{C\,IV} (C/H)_{\odot} 10^{[Z/H]}} \frac{Z_{\text{N}}}{Z_{\text{I}}} \quad (3)$$

where $f_{\text{C IV}} = N_{\text{C IV}}/N_{\text{C}}$ is the C IV ionization fraction, and Z_{N} and Z_{I} are shorthands for the absolute metallicities in the neutral and ionized gas. We have assumed a solar elemental abundance pattern, so that $[\text{C}/\text{H}] = [\text{Z}/\text{H}]$, and we take the solar carbon abundance $\text{C}/\text{H} = 10^{-3.61}$ from Allende Prieto et al. (2002). We assume that $Z_{\text{N}}/Z_{\text{I}} = 1$, though values <1 are possible in a scenario where metal-rich, ionized supernova ejecta has yet to mix with the general interstellar medium (ISM), and values >1 are possible in an accretion scenario. Finally, we assume that $f_{\text{C IV}} = 0.3$, since in Paper I we found this is the maximum amount allowed in *either* photoionization (Ferland et al. 1998) or collisional ionization (Gnat & Sternberg 2007) models, and so it gives the most conservative (lowest) value of $N_{\text{H II}}$. Lower values of $f_{\text{C IV}}$ would increase the $N_{\text{H II}}$ estimates.

The resulting values of $N_{\text{H II}}$ are shown in Fig. 8. Based on the 74 systems in this sample, we find that the mean and standard deviation of the warm ionized-to-neutral ratio is $\langle \log(N_{\text{H II}}/N_{\text{H I}}) \rangle = -1.0 \pm 0.6$, i.e. the C IV phase contains $>10\%$ of the baryons of the neutral phase. The sub-DLAs show a mean $\log N_{\text{H II}}$ of 19.33, whereas the DLAs show a mean $\log N_{\text{H II}}$ of 19.77, a factor of ≈ 2.2 higher. This is because sub-DLAs show (on average) similar C IV columns as DLAs, but higher metallicities. We note in the lower panel of Fig. 8 that there is no trend for $N_{\text{H II}}$, which is $\propto N_{\text{C IV}}/(\text{Z}/\text{H})$, to depend on metallicity (although such a trend could be partly hidden by the saturation of C IV in high metallicity systems). Thus, the correlation reported in Sect 3.4 between $N_{\text{C IV}}$ and $[\text{Z}/\text{H}]$ appears to be a simple consequence of the metallicity alone, but does not imply that there is more ionized gas (i.e. more H II) in the high-metallicity systems. We also note that the scatter in $N_{\text{H II}}$ is substantial, of order ≈ 2 dex in $N_{\text{H II}}$ at values of $[\text{Z}/\text{H}]$ between -2.0 and -1.0 .

3.10. C IV column density vs gas cooling rate

The cooling rate l_{c} in diffuse interstellar gas is directly proportional to the $N_{\text{C II}^*}/N_{\text{H I}}$ ratio¹, according to $l_{\text{c}} = N_{\text{C II}^*} h\nu_{\text{ul}} A_{\text{ul}}/N_{\text{H I}} \text{ erg s}^{-1}$ per H atom, where A_{ul} is the Einstein A coefficient and $h\nu_{\text{ul}}$ the energy of the $158 \mu\text{m}$ line (Pottasch 1979). The cooling rate is of interest since it is equivalent to the heating rate, because the cooling time is so shorter than the dynamical time (Wolfe et al. 2003a,b). In turn, the heating rate will be related to the intensity of UV radiation and the dust-to-gas ratio, and ultimately to the star formation rate per unit area.

We searched the literature for C II* measurements in our sample of DLAs/sub-DLAs with C IV. We took 20 data points (11 measurements and 9 upper limits) from Srianand et al. (2005), 9 measurements from Wolfe et al. (2003a), and one from Heinmüller et al. (2006). In Fig. 9, we directly compare the cooling rate with the C IV column density. Below $\log l_{\text{c}} = -26.8$, there is no trend evident in the data. However, we find that the seven points with the highest $N_{\text{C IV}}$ are among the systems with the highest cooling rate. Even though a formal correlation between the cooling rate and $N_{\text{C IV}}$ is detected only at the 1.8σ level (the C II* upper limits were excluded in this analysis), we

¹ C II* is an excited electronic state of singly ionized carbon. The transition at $158 \mu\text{m}$ resulting from the decay from fine-structure state $^2P_{3/2}$ to $^2P_{1/2}$ in the $2s^2 2p$ term of C^+ is the principal coolant for diffuse neutral interstellar gas.

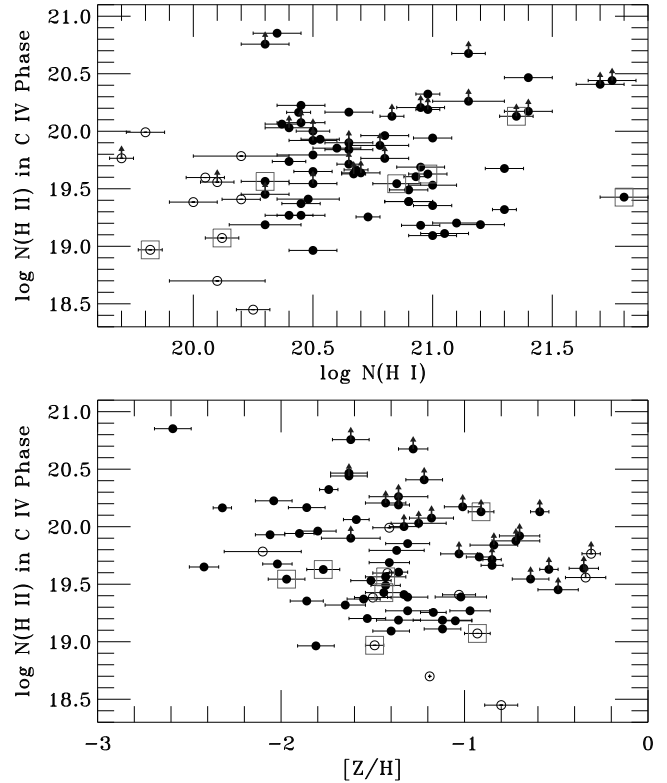


Fig. 8. Comparison of H II column density in the C IV-bearing gas integrated over all velocities with (top) $N_{\text{H I}}$ and (bottom) $[\text{Z}/\text{H}]$ for each system in our sample, assuming an ionization fraction $N_{\text{C IV}}/N_{\text{C}} = 0.3$. The average value of the ratio $N(\text{H II})/N(\text{H I})$ over all 74 systems is 0.1, implying that the C IV phase of DLAs and sub-DLAs typically contains $>10\%$ of the baryons and metals in the neutral phase. The mean value of $N_{\text{H II}}$ is ≈ 2.5 times lower in sub-DLAs than in DLAs.

note that the the median logarithmic C IV column density among the systems with $\log l_{\text{c}} < -26.8$ is 13.86, whereas the median among the systems with $\log l_{\text{c}} > -26.8$ is 14.83. This finding is consistent with the results of Wolfe (2007, in preparation), who finds evidence for bimodality in DLAs based on the cooling rate, in the form of significant differences between the metallicities and velocity widths of those DLAs with cooling rates below and above a critical value $l_{\text{c}} = 10^{-27} \text{ erg s}^{-1} \text{ H}^{-1}$.

4. Discussion

4.1. Narrow and broad components

There are two physical processes that can provide the 47.9 eV required to ionize C^{+2} to C^{+3} , and so create the gas seen in C IV: photoionization and collisional ionization. In Paper I it was shown [see Fig 3(b) in that paper] that the line widths of at least one fifth of the C IV components observed in DLAs are narrow ($b \lesssim 10 \text{ km s}^{-1}$), implying that in these components, the gas is cool ($T < 7 \times 10^4 \text{ K}$), which likely implies collisional ionization is unimportant, and that photoionization is the ionization mechanism². These nar-

² Cool but highly ionized clouds could however be produced by a non-equilibrium collisional ionization scenario, in which

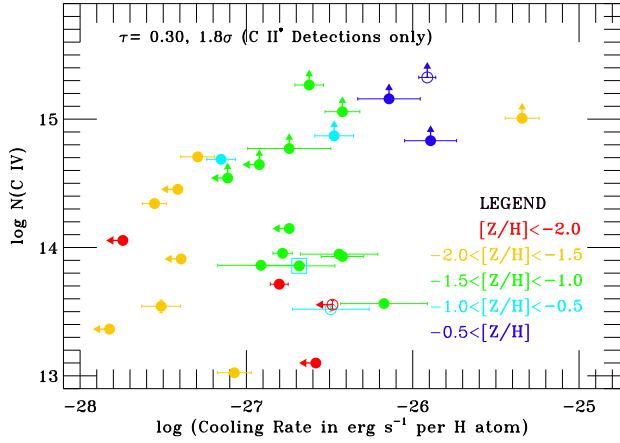


Fig. 9. Dependence of the C IV column density on the cooling rate, derived from the $N_{\text{C II}^*}/N_{\text{H I}}$ ratio, for each DLA (filled circles) and sub-DLA (open circles) where data on C IV and C II* exist. Color-coding is used to denote the metallicity of the gas, as indicated in the legend. The seven data points with the highest $N_{\text{C IV}}$ all show above-average cooling rates. Among these seven, six show high metallicities.

row components are not seen in O VI. The detection of cool C IV components rules out the idea that all the C IV in DLAs arises in a hot halo (see Mo & Miralda-Escudé 1996; Maller et al. 2003). The source of the extreme-ultraviolet (EUV) radiation at 259 Å that photoionizes C⁺ to C²⁺ and gives rise to the narrow C IV components could be external (the extragalactic background) or internal (O- and B- type stars in the DLA host galaxies). Discussions of the relative importance of internal and external radiation in DLAs are given by Howk & Sembach (1999), Miralda-Escudé (2005), and Schaye (2006). Note that in the Milky Way, Bregman & Harrington (1986) found that planetary nebulae are the dominant source of photons in the range 45–54 eV, but DLA galaxies at $z > 2$ are likely too young for planetary nebulae to have formed.

We propose that the broad C IV components arise in the hotter phase of DLA plasma that is detected in O VI absorption (Paper I), i.e. the hot ionized medium. This phase will arise following either heat input from supernova in the DLA host galaxy, or by the shock-heating of infalling gas at the virial radius. In the first case, the hot ionized medium may exist in the form of a wind (Oppenheimer & Davé 2006; Fangano et al. 2007; Kawata & Rauch 2007), though Galactic fountain scenarios are also possible (Shapiro & Field 1976; Bregman 1980; Houck & Bregman 1990). The observation that up to 80% of the C IV components are broad is consistent with the origin of the C IV in a wind, since in the models of Oppenheimer & Davé (2006), much of the C IV in galactic winds is collisionally ionized.

We note that Type II supernovae will heat interstellar gas to temperatures $> 10^6$ K, too high for the formation of O VI and C IV lines, and left to itself, gas at a density of 10^{-3} cm^{-3} and one-hundredth of the solar metallicity will not cool in a Hubble time. However, if the hot plasma

initially hot gas has cooled faster than it has recombined, leading to “frozen-in” ionization (Kafatos 1973).

interacts with cool or warm entrained clouds, conductive interfaces (Borkowski et al. 1990), turbulent mixing layers (Slavin et al. 1993; Esquivel et al. 2006), or shock fronts (Dopita & Sutherland 1996) can form between the hot and cool phases, in which the temperatures are favorable for the formation of O VI and C IV lines. These mechanisms, which have been invoked to explain high-ion observations in the extended halo of the Milky Way (Savage et al. 2003; Zsargó et al. 2003; Indebetouw & Shull 2004), in high-velocity clouds (Sembach et al. 2003; Fox et al. 2004, 2005; Collins et al. 2005), and in the Large Magellanic Cloud (Lehner & Howk 2007), can explain the broader C IV and O VI components seen in the DLAs and sub-DLAs. Note that the interpretation of broad high-ion components in DLAs and sub-DLAs as hot and collisionally ionized is different from the interpretation of the O VI components in the IGM at $z \gtrsim 2$, which (generally) appear to be photoionized (Carswell, Schaye, & Kim 2002; Bergeron et al. 2002; Levshakov et al. 2003; Bergeron & Herbert-Fort 2005; Reimers et al. 2006; Lopez et al. 2007), though see Reimers et al. (2001) and Simcoe et al. (2002, 2006).

4.2. Ionized gas and star formation

Ledoux et al. (2006) have presented a $[Z/H]$ - Δv_{Neut} correlation in DLAs and sub-DLAs, and have interpreted it as implying an underlying mass-metallicity relation (see also Wolfe & Prochaska 1998; Ledoux et al. 1998; Murphy et al. 2007; Prochaska et al. 2007a). In this interpretation, Δv_{Neut} traces motions due to gravity. Since we find that $\Delta v_{\text{C IV}}$ is larger than Δv_{Neut} in almost all cases, an additional energy source is required to heat and accelerate the C IV clouds. We suggest that star formation and subsequent supernovae could provide this source. Star formation in DLA and sub-DLA galaxies will lead to:

- (i) metals generated by stellar nucleosynthesis;
- (ii) EUV flux from OB stars that can photoionize C⁺ to C²⁺ in interstellar gas, giving rise to the narrow C IV components;
- (iii) supernovae-heated million-degree plasma, which can interact with entrained clouds of cooler gas to produce gas at $T \sim 10^5$ K, where O VI and C IV components are formed through electron collisions;
- (iv) mechanical energy injection from supernovae and stellar winds imparting large total velocity widths to the high ions.

Because star formation leads to metals and to feedback (i.e. mechanical energy injection into the ISM), this scenario would naturally explain the correlation between $[Z/H]$ and $\Delta v_{\text{C IV}}$. However, we cannot rule out an alternative scenario in which the plasma phases in DLAs and sub-DLAs are formed following the accretion of infalling, intergalactic gas, rather than by star formation (e.g. Wolfe & Prochaska 2000b). The inflow model can also qualitatively explain the metallicity-C IV line width correlation: the more massive halos (which through the mass-metallicity relationship tend to show higher metallicities) would induce higher accretion rates because of their deeper potential wells, and so could create and disperse the C IV over large velocity ranges.

4.3. Evidence for galactic outflows and winds

Our dataset shows that C IV components in DLAs and sub-DLAs exist over a broad velocity range, with a median $\Delta v_{\text{C IV}}$ of 187 km s^{-1} , which is approximately twice as broad as the typical velocity spread seen in the neutral gas. The terminal C IV velocities reach $>200 \text{ km s}^{-1}$ in 42/74 systems, and $>500 \text{ km s}^{-1}$ in 8/74 systems, and are correlated with the metallicity. Together, this evidence implies that the high ions in DLAs and sub-DLAs trace highly disturbed kinematic environments. In this section we identify a population of high-velocity C IV components with intriguing ionization properties, and we address whether these components could be created by galactic outflows.

In order to evaluate whether any of the observed C IV components represent winds, we need to determine the escape velocity in each system. We calculate this using $v_{\text{circ}} = \Delta v_{\text{Neut}}/0.6$, an empirical relation found from analysis of artificial spectra in the simulations of Haehnelt et al. (1998) and Maller et al. (2001). There is a factor of two dispersion around this relation, due to variations in the viewing angle. We then take $v_{\text{esc}} = \sqrt{2}v_{\text{circ}}$ (appropriate for a spherical halo), so that $v_{\text{esc}} \approx 2.4\Delta v_{\text{Neut}}$. The escape speed we have assumed can be taken as an upper limit, because v_{esc} is calculated in the disk and will decrease with radius, and we may be observing C IV at high radii. We have not accounted for drag forces arising due to entrainment between the winds and the galaxy's ISM (Finlator & Davé 2007).

When we search for C IV absorption at $v < -v_{\text{esc}}$ and $v > v_{\text{esc}}$, we find it in 25 of 63 DLAs and 4 of 11 sub-DLAs, i.e. C IV absorption unbound from the central potential well exists in $\approx 40\%$ of cases. These absorbers, which we refer to as wind candidates, are colored with dark shading in Fig. 1, for easy identification. A key property of the wind candidate absorbers is the low column density of the accompanying neutral gas absorption. In this respect, the wind candidates are analogous to the highly ionized high-velocity clouds seen in the vicinity of the Milky Way (Sembach et al. 1995, 1999, 2003; Collins et al. 2004, 2005; Fox et al. 2005, 2006; Ganguly et al. 2005). They also resemble the $z \approx 6$ C IV absorbers reported by Ryan Weber et al. (2006). In a handful of cases, wind candidates are seen at both redshifted and blueshifted velocities in the same system. In Fig. 10 (top panel) we plot the absolute wind C IV columns as a function of metallicity. We find similar C IV wind column densities in systems that span the 2.5 dex range of metallicity in our sample, even in the highest metallicity systems.

Our results are surprising when viewed in the light of simulations of galactic outflows, which show that dwarf galaxies are more important than massive galaxies for the metal pollution of the intergalactic medium (Mac-Low & Ferrara 1999; Ferrara et al. 2000; Nagamine et al. 2004b; Scannapieco et al. 2006b; Tissera et al. 2006; Kobayashi et al. 2007), since they are incapable of gravitationally confining the metals released by supernovae. The increase in wind escape fraction with decreasing galactic mass may contribute to the origin of the mass-metallicity relationship observed in DLAs and other high-redshift galaxies (Nagamine et al. 2004a; Tremonti et al. 2004; Møller et al. 2004; Savaglio et al.

2005; Erb et al. 2006)³. The surprising result here is that, given the mass-metallicity relation, the higher metallicity (higher mass) galaxies should decelerate their supernova-driven outflows, so that C IV outflows should not be seen in the high-metallicity systems, but yet we observe the high-velocity components even in systems with $[Z/H] > -1.0$. Furthermore, we find that the maximum outflow velocity v_{max} is correlated to the metallicity.

For any individual C IV component, it is difficult to determine conclusively whether one is seeing a galactic outflow from the DLA galaxy (see Fangano et al. 2007). Two other plausible origins are inflow toward the DLA galaxy (Wolfe & Prochaska 2000b), and the ISM of a separate nearby galaxy. A contribution of C IV from these processes could help to explain both the scatter seen in each panel in Figure 6, and the cases with large values for $\Delta v_{\text{C IV}}$. One weakness of the inflow model is that accretion would accelerate the gas up to but not beyond the escape velocity, but yet we see gas moving *above* the escape velocity. Thus inflow cannot explain the highest-velocity C IV components. The nearby galaxy model has the problem of not readily explaining why the ionized-to-neutral gas ratio is so high in the high-velocity C IV components. In other words, if nearby galaxies are responsible for the high-velocity C IV components, where is their neutral ISM? The outflow explanation, on the other hand, naturally explains the velocities and the ionization properties of the high-velocity C IV absorbers. The outflow model also explains the presence of metals in the ionized gas (they came from the DLA host galaxy), so it does not need to resort to pre-enrichment. A more serious problem is whether we can associate a single DLA with a single galaxy. This assumption may be false since the clustering of galaxies near DLAs has been observed both at low (Chen & Lanzetta 2003) and high (Cooke et al. 2006a,b; Bouché & Lowenthal 2003, 2004; Ellison et al. 2007) redshift. Our wind interpretation implicitly assumes that each high-velocity C IV component arose from a galaxy located in velocity at the point where the neutral line absorption is strongest.

4.3.1. Wind properties

We present in this section a calculation of order-of-magnitude estimates for the mass M , kinetic energy E_k , mass flow rate \dot{M} , and flux of kinetic energy \dot{E}_k in the C IV wind candidate absorbers. These calculations are analogous to those used to measure the energetics of winds in starburst galaxies (Heckman et al. 2000; Martin 2005, 2006) and LBGs (Pettini et al. 2000).

We assume that the outflow exists in an expanding hemispherical shell moving at velocity v relative to the neutral gas in the DLA galaxy (we do not assume a full spherical outflow, since we do not generally see two components corresponding to the near and far side of the galaxy). We then calculate M , E_k , \dot{M} , and \dot{E}_k using the following equations:

$$M = 2\pi r^2 \mu m_{\text{H}} N_{\text{H II}} \quad (4)$$

$$\dot{M} = 4\pi \mu m_{\text{H}} r |\dot{v}| N_{\text{H II}} \quad (5)$$

$$E_k = M \bar{v}^2 / 2 \quad (6)$$

³ Low star formation efficiency at low galactic masses may also contribute to the mass-metallicity relationship (Brooks et al. 2007; Finlator & Davé 2007).

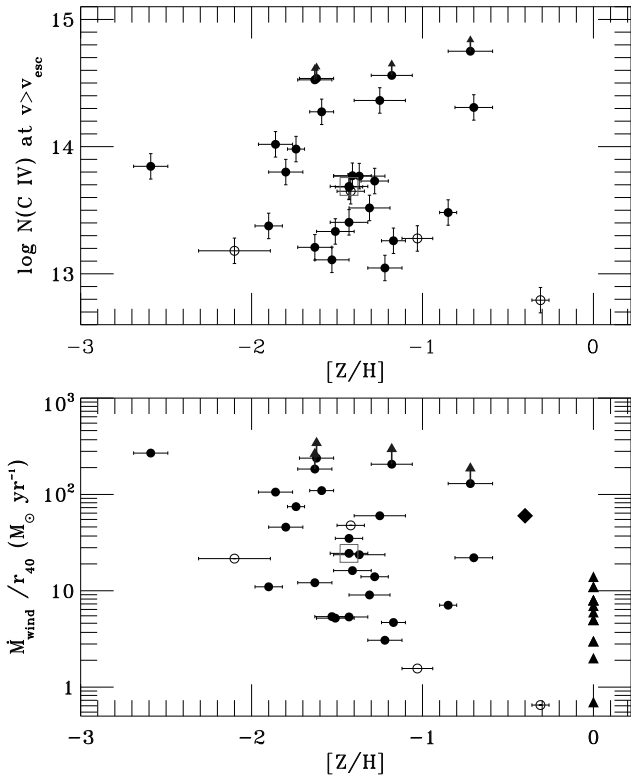


Fig. 10. **Top panel:** C IV column density moving above the escape speed (i.e. wind candidate $N_{\text{C IV}}$) as a function of metallicity, for the 25 DLAs and 4 sub-DLAs with C IV absorption at $|v| > |v_{\text{esc}}|$, where $v_{\text{esc}} = 2.4\Delta v_{\text{Neut}}$. **Bottom panel:** Wind mass outflow rate \dot{M}_{wind} divided by characteristic C IV radius r_{40} (in units of 40 kpc) vs metallicity. The median mass outflow rate among these cases is $22(r_{40}) M_{\odot} \text{ yr}^{-1}$. The large diamond shows the mass outflow rate determined in the $z = 2.7$ Lyman Break Galaxy cB58 by Pettini et al. (2000), assuming $r=1$ kpc. The filled triangles are the mass flow rates determined for the cool winds in the Martin (2006) sample of low-redshift ultraluminous starburst galaxies and plotted at zero metallicity for convenience. Only the DLA and sub-DLA points have been divided by r_{40} .

$$\dot{E}_k = \dot{M} \bar{v}^2 / 2 \quad (7)$$

Here $\mu = 1.3$ is the mean molecular weight, m_{H} is the mass of a hydrogen atom, and $N_{\text{H II}}$ is calculated using Eqn. 3. It can be seen that these four quantities are proportional to the zeroth, first, second, and third moments of the C IV optical depth profile. The wind mass flow rates are shown in the lower panel of Fig. 10. They were calculated by taking the average of the escape velocity and the terminal velocity for \bar{v} , and deriving $N_{\text{H II}}$ with Eqn. 3 only for that portion of the C IV absorption at $|v| > v_{\text{esc}}$. We only have information on the line-of-sight velocity (not the full 3D velocity), but since the line-of-sight passes through a DLA or sub-DLA, we assume we are looking through the full depth of the galactic halo, so that the line-of-sight velocity we measure approximates the radial velocity of the outflowing gas.

The only quantity which is not directly measured is the characteristic radius r . If we take a reference value of $r = 40$ kpc, as determined for C IV around LBGs by

Adelberger et al. (2005), we find that the 29 C IV wind candidates typically contain (median values) a total mass of $\sim 2 \times 10^9 M_{\odot}$, a kinetic energy of $\sim 1 \times 10^{57}$ erg, a mass flow rate of $\sim 22 M_{\odot} \text{ yr}^{-1}$, and a kinetic energy injection rate of $\sim 4 \times 10^{41} \text{ erg s}^{-1}$. To put these wind mass flow rates in perspective, Pettini et al. (2000, 2002) report a mass flow rate of $\approx 60 M_{\odot} \text{ yr}^{-1}$ for the outflow from the $z = 2.7$ LBG MS 1512-cB58, and Martin (2006) calculate the mass loss rates in the cool winds of a sample of low-redshift ultraluminous starburst galaxies as between 1 and $> 14 M_{\odot} \text{ yr}^{-1}$.

We calculate that the thermal energy in the C IV wind absorbers is only a few percent of their kinetic energy (assuming a temperature of 10^5 K). Assuming the clouds fill a region whose depth is similar to its width, a 40 kpc depth and $N_{\text{H II}} = 10^{20} \text{ cm}^{-2}$ correspond to a density of $n_{\text{H II}} \sim 10^{-3} \text{ cm}^{-3}$, assuming a filling factor of unity. In turn, such a medium would exhibit a thermal pressure $P/k \sim 10^2 \text{ cm}^{-3} \text{ K}$. If the C IV arose in interface layers between entrained cool/warm clouds and a surrounding hot gas, then the line-of-sight filling factor would be much lower and the C IV could exist in higher-density, higher-pressure, localized regions.

Among the 25 DLAs and 4 sub-DLAs showing wind candidate components, the median rate at which each galaxy delivers metals to the IGM is $\sim 1 \times 10^{-2} M_{\odot} \text{ yr}^{-1}$. This estimate is robust to changes in the metallicity of the ionized gas with respect to the neutral gas. Assuming that the outflows are driven by the supernovae that follow star formation, we can calculate the star formation rate necessary to power the observed C IV outflows. We use the relation from Efsthathiou (2000) between kinetic energy injection rate and star formation rate, $\dot{E}_{\text{SN}} = 2.5 \times 10^{41} \dot{M}_{\star} \text{ erg s}^{-1}$, with \dot{M}_{\star} in $M_{\odot} \text{ yr}^{-1}$. Equating \dot{E}_{SN} to the observed mean flux of kinetic energy, we find a median required SFR per DLA of $\sim 2 M_{\odot} \text{ yr}^{-1}$, corresponding (with our assumed $r = 40$ kpc) to a required SFR per unit area ($\dot{\psi}_{\star}$) of $\sim 3 \times 10^{-4} M_{\odot} \text{ yr}^{-1} \text{ kpc}^{-2}$. This is consistent with (though close to) the limit on the SFR per unit area derived from low surface brightness features (i.e. DLA analogs) in the Hubble Ultra-Deep Field by Wolfe & Chen (2006), who report $\dot{\psi}_{\star} \lesssim 10^{-3.6} M_{\odot} \text{ yr}^{-1} \text{ kpc}^{-2}$. We thus conclude that, at least to an order-of-magnitude, there is sufficient energy released following star formation to drive the observed high-velocity C IV components in DLAs, supporting the notion that they trace galactic winds.

5. Summary

We analyzed the C IV absorption in 63 DLAs and 11 sub-DLAs in the range $1.75 < z_{\text{abs}} < 3.61$ observed with VLT/UVES. We measured the properties of the C IV absorption in each system and investigated how they depend on the properties of the neutral gas. In most systems the metallicity, H I column density, and line width in the neutral gas had already been measured. We executed the neutral gas measurements for the remaining cases. This study has led us to find that:

1. The C IV absorption line profiles are complex, showing both narrow ($b < 10 \text{ km s}^{-1}$) and broad ($b > 10 \text{ km s}^{-1}$)

⁴ This relation assumes each supernova releases 10^{51} erg of kinetic energy and that one supernova follows from every 125 M_{\odot} of star formation.

- components, which trace cool, photoionized and hot, collisionally ionized gas, respectively (we used O VI to study the hot gas in Paper I).
2. The median C IV column densities in DLAs and sub-DLAs [$\log N_{\text{C IV}}(\text{DLA})=14.2$] are substantially higher than typical IGM values [$\log N_{\text{C IV}}(\text{IGM})=13.0$], but similar to those seen in LBGs [$\log N_{\text{C IV}}(\text{LBG})=14.0$].
 3. The total C IV line width is broader than the total neutral line width in 69 of 74 cases.
 4. The total C IV column density, line width, and velocity offset in the DLAs and sub-DLAs are all correlated, so the strongest C IV absorbers also tend to be the broadest and most offset relative to the neutral gas.
 5. The total C IV column density is correlated with the neutral-phase metallicity. The significance of this correlation is $>6.0\sigma$, and it is found even when the saturated cases, the proximate DLAs, and the sub-DLAs are excluded.
 6. The total C IV line width is weakly correlated with the neutral-phase metallicity. This correlation is detected at 4.1σ significance (using $(v_+ - v_-)_{\text{C IV}}$ to measure the total line width), and is found independently in the lower- and upper- redshift halves of the sample. The slope of the metallicity/high-ion line width relation is similar to the slope of the metallicity/low-ion line width relation reported by Ledoux et al. (2006).
 7. None of the C IV properties (column density, line width, central velocity) correlate with the H I column density, even though our sample spans a factor of 100 in $N_{\text{H I}}$. Indeed, though we only have 11 sub-DLAs against 63 DLAs, the mean values of $\log N$, Δv , and $|\bar{v}|$ are the same in DLAs as in sub-DLAs. However, assuming a constant ionization correction $N_{\text{C IV}}/N_{\text{C}} = 0.3$, then the sub-DLAs show a mean $N_{\text{H II}}$ of 19.36, whereas the DLAs show a mean $N_{\text{H II}}$ of 19.77, a factor of ≈ 2.5 higher. This is because sub-DLAs show (on average) similar C IV columns but higher metallicities.
 8. We find slightly lower mean C IV column densities and total line widths among the seven proximate DLAs/sub-DLAs than among the 67 intervening systems. This trend is worth investigating using a larger proximate sample.
 9. The mean velocity offset between the C IV and the neutral gas $|\bar{v}|_{\text{C IV}}$ has a mean value of 69 km s^{-1} over our 74 DLAs and sub-DLAs, implying a net amount of outflow or inflow is present. The maximum observed C IV velocity v_{max} reaches $>200 \text{ km s}^{-1}$ in 42/74 cases, and $>500 \text{ km s}^{-1}$ in eight cases. v_{max} is correlated with the metallicity at the 2.9σ level.
 10. We calculate the escape velocity from the width of the neutral line absorption. We observe C IV moving above the escape velocity in 25 DLAs and 4 sub-DLAs, covering 2.5 orders of magnitude of $[Z/H]$. In other words, C IV clouds that are unbound from the central potential well are seen in $\approx 40\%$ of DLAs and sub-DLAs. Assuming a characteristic C IV radius of 40 kpc, these wind candidate absorbers show typical (median) masses of $\sim 2 \times 10^9 M_{\odot}$, kinetic energies of $\sim 1 \times 10^{57} \text{ erg}$, mass flow rates of $\sim 22 M_{\odot} \text{ yr}^{-1}$, and kinetic energy injection rates $\dot{E}_k \sim 4 \times 10^{41} \text{ erg s}^{-1}$. The typical value for \dot{E}_k requires a SFR per DLA of $\sim 2 M_{\odot} \text{ yr}^{-1}$, or a SFR per unit area of $\sim 3 \times 10^{-4} M_{\odot} \text{ yr}^{-1} \text{ kpc}^{-2}$, to power the winds.

We conclude with several remarks concerning the origin of ionized gas in DLAs and sub-DLAs. Since $\Delta v_{\text{C IV}}$ is almost always broader than the gravitationally broadened Δv_{Neut} , an additional energy source is required to heat and accelerate the C IV-bearing clouds, in $\approx 40\%$ of cases to above to escape speed. We propose that star formation and supernovae can provide this source. DLA/sub-DLA galaxies with higher rates of star formation will produce higher EUV fluxes from massive stars, photoionizing the gas that is seen in the narrow C IV components, and will also undergo higher rates of Type II supernovae and stellar winds. The supernovae lead to (i) metal enrichment through nucleosynthesis, (ii) the generation of million-degree interstellar plasma, which can interact with embedded clouds to form gas containing C IV and O VI, and (iii) the injection of mechanical energy to the surrounding ISM, explaining the extended velocity fields for the ionized gas. Such a scenario would explain (at least qualitatively) the metallicity-C IV line width correlation, and the velocity and ionization level of the wind candidates.

Infalling clouds can also contribute to the C IV seen in DLAs (e.g. Wolfe & Prochaska 2000b). However, as we have pointed out, infall cannot explain the highest velocity C IV components, which are detected at well over the escape speed. Although metallicity measurements could in theory discriminate between the infall and outflow hypotheses, it is very difficult to directly measure the metallicity of the ionized gas in DLAs. However, one practical test of the idea that star formation leads to the production of ionized gas in DLAs (and the associated idea that the high-velocity C IV components in DLAs trace winds) would be a detailed comparison between the properties of C IV absorption in DLAs and in LBGs, where outflows are *directly* observed (Pettini et al. 2000, 2002; Shapley et al. 2003). Though we have not yet conducted a full comparison, we do note that the similar C IV column density distributions observed in DLAs and LBGs suggest that the ionized gas in these two classes of object shares a common origin in supernova-driven outflows.

Acknowledgements

AJF gratefully acknowledges the support of a Marie Curie Intra-European Fellowship awarded by the European Union Sixth Framework Programme. PP and RS gratefully acknowledge support from the Indo-French Centre for the Promotion of Advanced Research (Centre Franco-Indien pour la Promotion de la Recherche Avancée) under contract No. 3004-3. We thank Alain Smette for kindly providing the spectra of many quasars in the Hamburg-ESO survey prior to publication. We acknowledge valuable discussions with Blair Savage, Jason Prochaska, and Art Wolfe. Finally, we thank the referee for perceptive comments that improved the paper.

References

- Adelberger, K. L., Shapley, A. E., Steidel, C. C., Pettini, M., Erb, D. K., & Reddy, N. A., 2005, ApJ, 629, 636
- Aguirre, A., Hernquist, L., Schaye, J., Weinberg, D. H., Katz, N., & Gardner, J. 2001, ApJ, 560, 599
- Aguirre, A., Schaye, J., Hernquist, L., Kay, S., Springel, V., & Theuns, T. 2005, ApJ, 620, L13
- Akerman, C. J., Ellison, S. L., Pettini, M., & Steidel, C. C. 2005, A&A, 440, 499

- Allende Prieto, C., Lambert, D. L., & Asplund, A. 2002, *ApJ*, 573, L137
- Aracil, B., Petitjean, P., Pichon, C., & Bergeron, J. 2004, *A&A*, 419, 811
- Ballester, P., Modigliani, A., Boitquin, O., Cristiani, S., Hanuschik, R., Kaufer, A., & Wolf, S. 2000, *The Messenger*, 101, 31
- Bergeron, J., et al. 1994, *ApJ*, 436, 33
- Bergeron, J., Aracil, B., Petitjean, P., & Pichon, C. 2002, *A&A*, 396, L11
- Bergeron, J., & Herbert-Fort, S. 2005, *Probing Galaxies through Quasar Absorption Lines*, Proc. IAU 199, ed. Williams, Shu & Ménard, 265 (astro-ph/0506700)
- Boksenberg, A., Sargent, W. L. W., & Rauch, M. 2003, preprint (astro-ph/0307557)
- Borkowski, K. J., Balbus, S. A., & Fristrom, C. C. 1990, *ApJ*, 355, 501
- Bouché, N., & Lowenthal, J. D. 2003, *ApJ*, 596, 810
- Bouché, N., & Lowenthal, J. D. 2004, *ApJ*, 609, 513
- Bouché, N., Lehnert, M. D., & Péroux, C. 2005, *MNRAS*, 364, 319
- Bouché, N., Lehnert, M. D., & Péroux, C. 2006, *MNRAS*, 367, L16
- Bouché, N., Lehnert, M. D., Aguirre, A., Péroux, C., & Bergeron, J. 2007, *MNRAS*, 378, 525
- Bregman, J. N., & Harrington, J. P. 1986, *ApJ*, 309, 833
- Bregman, J. N. 1980, *ApJ*, 236, 577
- Brooks, A. M., Governato, F., Booth, C. M., Willman, B., Gardner, J. P., Wadsley, J., Stinson, G., & Quinn, T. 2007, *ApJ*, 655, L17
- Carswell, B., Schaye, J., & Kim, T.-S. 2002, *ApJ*, 578, 43
- Chen, H.-W., & Lanzetta, K. 2003, *ApJ*, 597, 706
- Collins, J. A., Shull, J. M., & Giroux, M. L. 2004, *ApJ*, 605, 216
- Collins, J. A., Shull, J. M., & Giroux, M. L. 2005, *ApJ*, 623, 196
- Cooke, J., Wolfe, A. M., Gawiser, E., & Prochaska, J. X. 2006a, *ApJ*, 636, L9
- Cooke, J., Wolfe, A. M., Gawiser, E., & Prochaska, J. X. 2006b, *ApJ*, 652, 992
- Cowie, L. L., & Songaila, A. 1998, *Nature*, 394, 44
- Davé, R., Hernquist, L., Katz, N., & Weinberg, D. H. 2000, *ApJ*, 539, 517
- Dekker, H., D’Odorico, S., Kaufer, A., Delabre, B., & Kotzlowski, H. 2000, *SPIE*, 4008, 534
- Dessauges-Zavadsky, M., Proux, C., Kim, T.-S., D’Odorico, S., & McMahon, R. G. 2003, *MNRAS*, 345, 447
- Dopita, M. A., & Sutherland, R. S. 1996, *ApJS*, 102, 161
- Efstathiou, G. 2000, *MNRAS*, 317, 697
- Ellison, S. L., Songaila, A., Schaye, J., & Pettini, M., 2000, *AJ*, 120, 1175
- Ellison, S. L., & Lopez, S. 2001, *A&A*, 380, 117
- Ellison, S. L., Yan, L., Hook, I. M., Pettini, M., Wall, J. V., & Shaver, P. 2002, *A&A*, 383, 91
- Ellison, S. L., Hennawi, J. F., Martin, C. L., & Sommer-Larsen, J. 2007, *MNRAS*, submitted (astro-ph/0704.1816)
- Erb, D. K., Shapley, A. E., Pettini, M., Steidel, C. C., Reddy, N. A., & Adelberger, K. L. 2006, *ApJ*, 644, 813
- Esquivel, A., Benjamin, R. A., Lazarian, A., Cho, J., & Leitner, S. N. 2006, *ApJ*, 648, 1043
- Fangano, A. P. M., Ferrara, A., & Richter, P. 2007, *MNRAS*, submitted (astro-ph/0704.2143)
- Ferland, G. J., Korista, K. T., Verner, D. A., Ferguson, J. W., Kingdon, J. B., & Verner, E. M. 1998, *PASP*, 110, 761
- Ferrara, A., Pettini, M., & Shchekinov, Y. 2000, *MNRAS*, 319, 539
- Ferrara, A., Scannapieco, E., & Bergeron, J. 2005, *ApJ*, 634, L37
- Finlator, K., & Davé, R. 2007, *MNRAS*, submitted (astro-ph/0704.3100)
- Fox, A. J., Savage, B. D., Wakker, B. P., Richter, P., Sembach, K. R., & Tripp, T. M. 2004, *ApJ*, 602, 738
- Fox, A. J., Wakker, B. P., Savage, B. D., Sembach, K. R., Tripp, T. M., & Bland-Hawthorn, J. 2005, *ApJ*, 630, 332
- Fox, A. J., Savage, B. D., & Wakker, B. P. 2006, *ApJS*, 165, 229
- Fox, A. J., Petitjean, P., Ledoux, C., & Srianand, R. 2007, *A&A*, 465, 171 (Paper I)
- Ganguly, R., Sembach, K. R., Tripp, T. M., & Savage, B. D. 2005, *ApJS*, 157, 251
- Gnat, O., & Sternberg, A. 2007, *ApJS*, 168, 213
- Haehnelt, M. G., Steinmetz, M., & Rauch, M. 1998, *ApJ*, 495, 647
- Heckman, T. M., Lehnert, M. D., Strickland, D. K., & Armus, L. 2000, *ApJS*, 129, 493
- Heckman, T. M., Sembach, K. R., Meurer, G. R., Strickland, D. K., Martin, C. L., Calzetti, D., & Leitherer, C. 2001, *ApJ*, 554, 1021
- Heinmüller, J., Petitjean, P., Ledoux, C., Caucci, S., & Srianand, R. 2006, *A&A*, 449, 33
- Hennawi, J. F. & Prochaska, J. X. 2007, *ApJ*, 655, 735
- Houck, J. C., & Bregman, J. N. 1990, *ApJ*, 352, 506
- Howk, J. C., & Sembach, K. R. 1999, *ApJ*, 523, L141
- Indebetouw, R., & Shull, J. M. 2004, *ApJ*, 607, 309
- Kafatos, M. 1973, *ApJ*, 182, 433
- Kawata, D., & Rauch, M. 2007, *ApJ*, submitted (astro-ph/0704.0652)
- Khare, P., Kulkarni, V. P., Péroux, C., York, D. G., Lauroesch, J. T., & Meiring, J. D. 2007, *A&A*, 464, 487
- Kirkman, D., & Tytler, D. 1997, *ApJ*, 489, L123
- Kirkman, D., & Tytler, D. 1999, *ApJ*, 512, L5
- Kobayashi, C., Springel, V., & White, S. D. M. 2007, *MNRAS*, 376, 1465
- Kulkarni, V. P., Khare, P., Péroux, C., York, D. G., Lauroesch, J. T., Meiring, J. D. 2007, *ApJ*, 661, L88
- Ledoux, C., Petitjean, P., Bergeron, J., Wampler, E. J., & Srianand, R. 1998, *A&A*, 337, 51
- Ledoux, C., Petitjean, P., & Srianand, R. 2003, *MNRAS*, 346, 209
- Ledoux, C., Petitjean, P., Fynbo, J. P. U., Møller, P., & Srianand, R. 2006, *A&A*, 457, 71
- Lehner, N., & Howk, J. C. 2007, *MNRAS*, 377, 687
- Levshakov, S. A., Agafonova, I. I., Reimers, D., & Baade, R. 2003, *A&A*, 404, 449
- Lopez, S., Ellison, S., D’Odorico, S., & Kim, T.-S. 2007, *A&A*, 469, 61
- Lu, L., Sargent, W. L. W., Barlow, T. A., Churchill, C. W., & Vogt, S. S. 1996, *ApJS*, 107, 475
- Mac Low, M., & Ferrara, A. 1999, *ApJ*, 513, 142
- Maller, A. H., Prochaska, J. X., Somerville, R. S., & Primack, J. R. 2001, *MNRAS*, 326, 1475
- Maller, A. H., Prochaska, J. X., Somerville, R. S., & Primack, J. R. 2003, *MNRAS*, 343, 268
- Martin, C. L. 2005, *ApJ*, 621, 227
- Martin, C. L. 2006, *ApJ*, 647, 222
- Miralda-Escudé, J. 2005, *ApJ*, 620, L91
- Mo, H. J., & Miralda-Escudé, J. 1996, *ApJ*, 469, 589
- Møller, P., Fynbo, J. P. U., & Fall, S. M. 2004, *A&A*, 422, L33
- Morton, D. C. 2003, *ApJS*, 149, 205
- Murphy, M. T., Curran, S. J., Webb, J. K., Ménager, H., & Zych, B. J., 2007, *MNRAS*, 376, 673
- Nagamine, K., Springel, V., & Hernquist, L. 2004a, *MNRAS*, 348, 421
- Nagamine, K., Springel, V., & Hernquist, L. 2004b, *MNRAS*, 348, 435
- Noterdaeme, P., Ledoux, C., Petitjean, P., Le Petit, F., Srianand, R., & Smette, A. 2007, *A&A*, in press (astro-ph/0707.4479)
- Oppenheimer, B., & Davé, R. 2006, *MNRAS*, 373, 1265
- Péroux, C., Dessauges-Zavadsky, M., D’Odorico, S., Kim, T.-S., & McMahon, R. G. 2003, *MNRAS*, 345, 480
- Péroux, C., Dessauges-Zavadsky, M., D’Odorico, S., Kim, T.-S., & McMahon, R. G. 2003, *MNRAS*, 363, 479
- Péroux, C., Dessauges-Zavadsky, M., D’Odorico, S., Kim, T.-S., & McMahon, R. G. 2007, *MNRAS*, in press (astro-ph/0707.2697)
- Petitjean, P., & Aracil, B. 2004, *A&A*, 422, 523
- Pettini, M. 1999, in Proc. ESO Workshop, Chemical Evolution from Zero to High Redshift, ed. J. R. Walsh & M. R. Rosa (Berlin: Springer), 233 (astro-ph/9902173)
- Pettini, M., Steidel, C. C., Adelberger, K. L., Dickinson, M., & Giavalisco, M. 2000, *ApJ*, 528, 96
- Pettini, M., Rix, S. A., Steidel, C. C., Adelberger, K. L., Hunt, M. P., & Shapley, A. E. 2002, *ApJ*, 569, 742
- Pottasch, S. R., Wesselius, P. R., & van Duinen, R. J. 1979, *A&A*, 74, L15
- Prochaska, J. X., & Wolfe, A. M. 1997, *ApJ*, 487, 73
- Prochaska, J. X., & Wolfe, A. M. 2002, *ApJ*, 566, 68
- Prochaska, J. X., Chen, H.-W., Wolfe, A. M., Dessauges-Zavadsky, M., Bloom, J. S. 2007a, *ApJ*, submitted (astro-ph/0703701)
- Prochaska, J. X., Hennawi, J. F., & Herbert-Fort, S. 2007b, *ApJ*, submitted (astro-ph/0703594)
- Reimers, D., Baade, R., Hagen, H.-J., & Lopez, S. 2001, *A&A*, 374, 871
- Reimers, D., Agafonova, I. I., Levshakov, S. A., Hagen, H.-J., Fechner, C., Tytler, D., Kirkman, D., & Lopez, S. 2006, *A&A*, 449, 9
- Richter, P., Ledoux, C., Petitjean, P., & Bergeron, J. 2005, *A&A*, 440, 819
- Russell, D. M., Ellison, S. L., & Benn, C. R. 2006, *MNRAS*, 367, 412
- Ryan-Weber, E. V., Pettini, M., & Madau, P. 2006, *MNRAS*, 371, L78
- Savage, B. D., & Sembach, K. R. 1991, *ApJ*, 379, 245

- Savaglio, S., et al. 2005, 635, 260, ApJ,
 Savage, B. D., et al. 2003, ApJS, 146, 125
 Scannapieco, E., Pichon, C., Aracil, B., Petitjean, P., Thacker, R. J.,
 Pogosyan, D., Bergeron, J., & Couchman, H. M. P. 2006a, MNRAS,
 365, 615
 Scannapieco, C., Tissera, P. B., White, S. D. M., & Springel, V. 2006b,
 MNRAS, 371, 1125
 Schaye, J., Aguirre, A., Kim, T.-S., Theuns, T., Rauch, M., & Sargent,
 W. L. W. 2003, ApJ, 593, 768
 Schaye, J. 2006, ApJ, 643, 59
 Schaye, J., Carswell, R. F., & Kim, T.-S. 2007, MNRAS, submitted
 (astro-ph/0701761)
 Sembach, K. R., Savage, B. D., Lu, L., & Murphy, E. M. 1995, ApJ,
 451, 616
 Sembach, K. R., & Savage, B. D., Lu, L., & Murphy, E. M. 1999,
 ApJ, 515, 108
 Sembach, K. R., et al. 2003, ApJS, 146, 165
 Shapiro, P. R., & Field, G. B. 1976, ApJ, 205, 762
 Shapley, A. E., Steidel, C. C., Pettini, M., & Adelberger, K. L. 2003,
 ApJ, 588, 65
 Simcoe, R. A., Sargent, W. L. W., & Rauch, M. 2002, ApJ, 578, 737
 Simcoe, R. A., Sargent, W. L. W., Rauch, M., & Becker, G. 2006,
 ApJ, 637, 648
 Slavin, J. D., Shull, J. M., & Begelman, M. C. 1993, ApJ, 407, 83
 Smette, A., Wisotzki, L., Ledoux, C., Garcet, O., Lopez, S.,
 & Reimers, D. et al. 2005, Probing Galaxies through Quasar
 Absorption Lines, Proc. IAU 199, ed. Williams, Shu, & Ménard,
 475 (astro-ph/0504657)
 Sommer-Larsen, J., & Fynbo, J. P. U. 2007, MNRAS, submitted
 (astro-ph/0703698)
 Songaila, A. 2005, AJ, 130, 1996
 Songaila, A. 2006, AJ, 131, 24
 Srianand, R., Petitjean, P., Ledoux, C., Ferland, G. & Shaw, G. 2005,
 MNRAS, 362, 549
 Strickland, D. K., Heckman, T. M., Colbert, E. J. M., Hoopes, C. G.,
 & Weaver, K. A. 2004, ApJ, 606, 829
 Tissera, P. B., Scannapieco, C., White, S. D. M., & Springel, V. 2006,
 Revista Mexicana de Astronomía y Astrofísica, 26, 125
 Tremonti, C. A., et al. 2004, ApJ, 613, 898
 Veilleux, S., Cecil, G., Bland-Hawthorn, J. 2005, ARA&A, 43, 769
 Wolfe, A. M., Gawiser, E., & Prochaska, J. X. 2005, ARA&A, 43, 861
 Wolfe, A. M., & Prochaska, J. X. 1998, ApJ, 494, L15
 Wolfe, A. M., & Prochaska, J. X. 2000a, ApJ, 545, 591
 Wolfe, A. M., & Prochaska, J. X. 2000b, ApJ, 545, 603
 Wolfe, A. M., Prochaska, J. X., & Gawiser, E. 2003a, ApJ, 593, 215
 Wolfe, A. M., Gawiser, E., & Prochaska, J. X. 2003b, ApJ, 593, 235
 Wolfe, A. M., & Chen, H.-W. 2006, ApJ, 652, 981
 Zsargó, J., Sembach, K. R., Howk, J. C., & Savage, B. D. 2003, ApJ,
 586, 1019

Table 1. Comparison of C IV and Neutral DLA Measurements

| QSO | z_{em} | z_{abs}^1 | Neutral Gas Properties ² | | | | C IV Properties | | | |
|-----------|-----------------|--------------------|-------------------------------------|------------|----|----------------------------|-------------------|--------------------------|----------------------------|---------------------------|
| | | | $\log N_{\text{H I}}$ | [Z/H] | Z | Δv_{Neut}^3 | Line ⁴ | $\log N_{\text{C IV}}^5$ | $\Delta v_{\text{C IV}}^6$ | $\bar{v}_{\text{C IV}}^7$ |
| Q0010-002 | 2.15 | 2.02478 | 20.95±0.10 | -1.43±0.11 | Zn | 32 | 1550 | >14.65 | <110 | -15±6 |
| Q0013-004 | 2.09 | 1.97295 | 20.83±0.05 | -0.59±0.05 | Zn | 720 | 1550 ⁸ | >15.41 | <1111 | -42±40 |
| Q0027-186 | 2.56 | 2.40186 | 21.75±0.10 | -1.63±0.10 | Zn | 44 | 1550 | >14.68 | <227 | 104±6 |
| Q0039-339 | 2.48 | 2.22400 | 20.60±0.10 | -1.31±0.12 | Si | 122 | 1550 | 14.41±0.01 | 168±3 | 39±3 |
| Q0042-295 | 2.39 | 1.80947 | 20.40±0.10 | -1.25±0.15 | Si | 65 | 1550 | >14.65 | <200 | -137±8 |
| Q0049-283 | 2.26 | 1.88615 | 20.20±0.08 | -1.03±0.09 | S | 26 | 1550 | 14.25±0.02 | 123±4 | -3±3 |
| Q0049-283 | 2.26 | 2.07125 | 20.45±0.10 | -1.31±0.12 | Si | 51 | 1548 | 13.83±0.02 | 229±3 | 110±5 |
| Q0058-292 | 3.09 | 2.67140 | 21.10±0.10 | -1.53±0.10 | Zn | 34 | 1548 | 13.54±0.05 | 293±13 | -68±17 |
| Q0102-190 | 3.04 | 2.36962 | 21.00±0.08 | -1.90±0.08 | S | 17 | 1550 | 13.91±0.02 | 123±3 | -19±3 |
| Q0102-190 | 3.04 | 2.92650 | 20.00±0.10 | -1.50±0.10 | Si | 146 | 1548 | 13.75±0.01 | 172±3 | 47±3 |
| Q0112+029 | 2.81 | 2.42310 | 20.90±0.10 | -1.31±0.11 | S | 112 | 1548 | 13.95±0.01 | 161±3 | 27±3 |
| Q0112-306 | 2.99 | 2.41850 | 20.50±0.08 | -2.42±0.08 | Si | 31 | 1548 | 13.10±0.02 | 35±3 | 6±3 |
| Q0112-306 | 2.99 | 2.70230 | 20.30±0.10 | -0.49±0.11 | Si | 218 | 1550 | >14.83 | <295 | -22±6 |
| Q0135-273 | 3.21 | 2.10739 | 20.30±0.15 | -1.12±0.16 | S | 92 | 1548 | 13.94±0.01 | 88±3 | 47±3 |
| Q0135-273 | 3.21 | 2.80003 | 21.00±0.10 | -1.40±0.10 | S | 66 | 1548 | 13.56±0.02 | 153±3 | 0±3 |
| Q0216+080 | 2.99 | 2.29306 | 20.50±0.10 | -0.70±0.11 | Zn | 104 | 1550 | >15.09 | <399 | -51±12 |
| Q0254-404 | 2.28 | 2.04607 | 20.45±0.08 | -1.55±0.09 | S | 37 | 1548 | 13.69±0.01 | 111±3 | 0±3 |
| Q0300-318 | 2.37 | 2.17905 | 20.80±0.10 | -1.80±0.10 | S | 41 | 1548 | 14.03±0.02 | 211±3 | -96±4 |
| Q0331-451 | 2.67 | 2.65618 | 19.82±0.05 | -1.49±0.05 | Si | 80 | 1548 | 13.35±0.01 | 81±3 | -88±3 |
| Q0347-383 | 3.22 | 3.02485 | 20.73±0.05 | -1.17±0.07 | Zn | 93 | 1548 | 13.95±0.01 | 319±3 | -35±3 |
| Q0405-443 | 3.02 | 1.91270 | 20.80±0.10 | -1.03±0.10 | Zn | 98 | 1550 | >14.60 | <205 | -42±6 |
| Q0405-443 | 3.02 | 2.54990 | 21.15±0.15 | -1.36±0.16 | Zn | 165 | 1550 | >14.77 | <187 | 83±12 |
| Q0405-443 | 3.02 | 2.59475 | 21.05±0.10 | -1.12±0.10 | Zn | 79 | 1548 | 13.86±0.01 | 131±3 | 31±3 |
| Q0405-443 | 3.02 | 2.62140 | 20.45±0.10 | -2.04±0.10 | Si | 182 | 1548 | 14.06±0.01 | 231±3 | 109±3 |
| Q0421-264 | 2.28 | 2.15680 | 20.65±0.10 | -1.86±0.10 | Si | 47 | 1548 | 14.18±0.01 | 227±3 | 152±3 |
| Q0425-522 | 2.25 | 2.22430 | 20.30±0.10 | -1.43±0.11 | S | 40 | 1548 | 14.00±0.01 | 435±3 | 156±5 |
| Q0438-436 | 2.86 | 2.34736 | 20.78±0.12 | -0.72±0.13 | Zn | 89 | 1550 ⁸ | >15.03 | <1035 | -425±40 |
| Q0458-020 | 2.29 | 2.03955 | 21.70±0.10 | -1.22±0.10 | Zn | 88 | 1550 | >15.06 | <185 | -63±46 |
| Q0528-250 | 2.77 | 2.14105 | 20.98±0.05 | -1.36±0.06 | Zn | 105 | 1550 | >14.70 | <113 | -51±12 |
| Q0528-250 | 2.77 | 2.81115 | 21.35±0.07 | -0.91±0.07 | Zn | 304 | 1550 | >15.09 | <188 | -4±12 |
| Q0551-366 | 2.32 | 1.96221 | 20.70±0.08 | -0.35±0.08 | Zn | 468 | 1548 | >15.16 | <461 | -121±38 |
| Q0642-506 | 3.09 | 2.65860 | 20.95±0.08 | -1.05±0.09 | Zn | 99 | 1548 | 14.00±0.01 | 168±3 | 15±3 |
| Q0841+129 | 2.50 | 1.86388 | 21.00±0.10 | -1.51±0.11 | S | 32 | 1548 | 13.89±0.01 | 126±3 | -33±3 |
| Q0913+072 | 2.78 | 2.61840 | 20.35±0.10 | -2.59±0.10 | Si | 22 | 1548 | 14.13±0.01 | 175±3 | 76±3 |
| Q1036-229 | 3.13 | 2.77739 | 20.93±0.05 | -1.36±0.05 | S | 80 | 1550 | 14.11±0.01 | 133±3 | 90±3 |
| Q1037-270 | 2.20 | 2.13906 | 19.70±0.05 | -0.31±0.05 | Zn | 250 | 1550 | >15.32 | <496 | -125±12 |
| Q1108-077 | 3.92 | 3.60760 | 20.37±0.07 | -1.59±0.07 | Si | 31 | 1548 | 14.34±0.01 | 410±3 | -108±3 |
| Q1111-152 | 3.37 | 3.26548 | 21.30±0.05 | -1.65±0.11 | Zn | 140 | 1548 | 13.54±0.01 | 149±3 | 101±3 |
| Q1117-134 | 3.96 | 3.35037 | 20.95±0.10 | -1.41±0.11 | Zn | 44 | 1548 | 14.15±0.01 | 233±3 | 46±3 |
| Q1157+014 | 1.99 | 1.94375 | 21.80±0.10 | -1.44±0.10 | Zn | 89 | 1548 | 13.86±0.01 | 102±3 | -9±3 |
| Q1203+023 | 2.13 | 1.74735 | 20.40±0.10 | -0.97±0.11 | Zn | 38 | 1550 | 14.17±0.01 | 77±3 | -36±3 |
| Q1209+093 | 3.30 | 2.58440 | 21.40±0.10 | -1.01±0.10 | Zn | 214 | 1550 | >15.03 | <355 | -34±20 |
| Q1220-180 | 2.16 | 2.11285 | 20.12±0.07 | -0.93±0.07 | S | 95 | 1548 | 14.01±0.01 | 119±3 | 3±3 |
| Q1223+178 | 2.94 | 2.46608 | 21.40±0.10 | -1.63±0.10 | Zn | 91 | 1550 | 14.71±0.01 | 320±3 | 18±3 |
| Q1232+082 | 2.57 | 2.33771 | 20.90±0.08 | -1.43±0.08 | S | 85 | 1548 | 13.93±0.01 | 653±3 | 246±4 |
| Q1242+001 | 2.08 | 1.82452 | 20.45±0.10 | -1.18±0.12 | Zn | 56 | 1550 ⁸ | >14.76 | <900 | -400±40 |
| Q1331+170 | 2.08 | 1.77635 | 21.15±0.07 | -1.28±0.08 | Zn | 75 | 1550 | >15.27 | <308 | -24±12 |
| Q1337+113 | 2.92 | 2.79583 | 21.00±0.08 | -1.86±0.09 | Si | 42 | 1548 | 13.36±0.03 | 78±4 | -29±4 |
| Q1340-136 | 3.20 | 3.11835 | 20.05±0.08 | -1.42±0.08 | S | 153 | 1550 ⁸ | 14.05±0.05 | 1044±20 | 180±20 |
| Q1409+095 | 2.85 | 2.01882 | 20.65±0.10 | -1.62±0.16 | Zn | 39 | 1548 | >14.15 | < 93 | -20±6 |
| Q1409+095 | 2.85 | 2.45595 | 20.53±0.08 | -2.06±0.08 | Si | 69 | 1548 | 13.74±0.01 | 74±3 | 15±3 |
| Q1409+095 | 2.85 | 2.66818 | 19.80±0.08 | -1.41±0.09 | S | 100 | 1550 | 14.45±0.01 | 172±3 | -102±3 |
| Q1444+014 | 2.21 | 2.08679 | 20.25±0.07 | -0.80±0.09 | Zn | 294 | 1548 | 13.52±0.02 | 305±5 | 63±5 |
| Q1451+123 | 3.25 | 3.17081 | 20.20±0.20 | -2.10±0.21 | Si | 45 | 1548 | 13.55±0.03 | 115±5 | 112±11 |
| Q2059-360 | 3.09 | 3.08291 | 20.98±0.08 | -1.77±0.09 | S | 44 | 1548 | 13.73±0.01 | 103±3 | 39±3 |
| Q2116-358 | 2.34 | 1.99618 | 20.10±0.07 | -0.34±0.11 | Zn | 177 | 1550 | >15.09 | <231 | 49±12 |
| Q2138-444 | 3.17 | 2.85235 | 20.98±0.05 | -1.74±0.05 | Zn | 60 | 1548 | 14.45±0.01 | 342±3 | -67±3 |
| Q2152+137 | 4.26 | 3.31600 | 20.50±0.15 | -1.37±0.15 | Si | 74 | 1548 | 14.29±0.01 | 389±3 | -66±3 |
| Q2206-199 | 2.56 | 1.91998 | 20.67±0.05 | -0.54±0.05 | Zn | 136 | 1548 | >14.96 | <195 | 57±12 |

Table 2. Statistical Significance of Correlations: Kendall τ Analysis

| Quan. 1 | Quan. 2 | Sample | Size | τ | σ |
|---------------------------|-----------------------------|--------------------------|------|--------|----------|
| $N_{\text{C IV}}$ | $(v_+ - v_-)_{\text{C IV}}$ | all | 74 | 0.54 | >6.0 |
| | | interv DLA ^a | 58 | 0.52 | >6.0 |
| | | unsaturated ^b | 49 | 0.45 | 4.5 |
| $ \bar{v} _{\text{C IV}}$ | $(v_+ - v_-)_{\text{C IV}}$ | all | 74 | 0.34 | 4.3 |
| | | interv DLA | 58 | 0.35 | 3.8 |
| $[\text{Z}/\text{H}]$ | $N_{\text{C IV}}$ | all | 74 | 0.45 | >6.0 |
| | | interv DLA | 58 | 0.46 | 5.1 |
| | | Zn II ^c | 37 | 0.40 | 3.5 |
| | | unsaturated | 49 | 0.25 | 2.5 |
| $[\text{Z}/\text{H}]$ | $\Delta v_{\text{C IV}}$ | all | 74 | 0.28 | 3.4 |
| | | interv DLA | 58 | 0.27 | 2.9 |
| | | Zn II | 37 | 0.30 | 2.6 |
| | | unsaturated | 49 | 0.14 | 1.4 |
| $[\text{Z}/\text{H}]$ | $(v_+ - v_-)_{\text{C IV}}$ | all | 74 | 0.33 | 4.1 |
| | | interv DLA | 58 | 0.30 | 3.3 |
| | | Zn II | 37 | 0.29 | 2.5 |
| | | $z < 2.34$ | 37 | 0.39 | 3.3 |
| | | $z > 2.34$ | 37 | 0.34 | 2.9 |
| $[\text{Z}/\text{H}]$ | $v_{\text{max, C IV}}$ | all | 74 | 0.24 | 2.9 |
| | | interv DLA | 58 | 0.24 | 2.6 |
| | | Zn II | 37 | 0.22 | 1.9 |
| $N_{\text{C IV}}$ | l_{c} | C II* detected | 21 | 0.30 | 1.9 |

^a In the intervening DLA sample, sub-DLAs and DLAs at $< 5000 \text{ km s}^{-1}$ from the QSO were excluded.

^b In the unsaturated sample (considered for correlations involving $N_{\text{C IV}}$ or $\Delta v_{\text{C IV}}$), all saturated C IV lines were removed.

^c In the Zn II sample, cases where $[\text{Z}/\text{H}]$ was derived from Si or S were excluded. This only applies to correlations involving $[\text{Z}/\text{H}]$.

Table 1. continued.

| QSO | z_{em} | z_{abs}^1 | Neutral Gas Properties ² | | | | C IV Properties | | | |
|-----------|-----------------|--------------------|-------------------------------------|-----------------------|----|----------------------------|-------------------|--------------------------|----------------------------|---------------------------|
| | | | $\log N_{\text{H I}}$ | $[\text{Z}/\text{H}]$ | Z | Δv_{Neut}^3 | Line ⁴ | $\log N_{\text{C IV}}^5$ | $\Delta v_{\text{C IV}}^6$ | $\bar{v}_{\text{C IV}}^7$ |
| Q2206–199 | 2.56 | 2.07622 | 20.44±0.05 | −2.32±0.05 | Si | 20 | 1548 | 13.71±0.01 | 47±3 | 3±3 |
| Q2222–396 | 2.18 | 2.15387 | 20.85±0.10 | −1.97±0.10 | S | 21 | 1548 | 13.44±0.02 | 49±3 | −3±3 |
| Q2228–399 | 2.21 | 2.09437 | 21.20±0.10 | −1.36±0.12 | Zn | 138 | 1548 | 13.70±0.02 | 186±5 | 43±5 |
| Q2243–605 | 3.01 | 2.33061 | 20.65±0.05 | −0.85±0.05 | Zn | 173 | 1550 | >14.73 | <349 | −272±14 |
| Q2311–373 | 2.48 | 2.18210 | 20.48±0.13 | < −1.33 | Zn | 77 | 1548 | 13.95±0.01 | 127±3 | −36±3 |
| Q2314–409 | 2.45 | 1.85733 | 20.90±0.10 | −1.02±0.14 | Zn | 95 | 1548 | 14.24±0.01 | 143±3 | −24±3 |
| Q2314–409 | 2.45 | 1.87519 | 20.10±0.20 | < −1.19 | Zn | 49 | 1548 | 13.38±0.02 | 140±4 | 37±4 |
| Q2318–111 | 2.96 | 1.98888 | 20.68±0.05 | −0.85±0.06 | Zn | 207 | 1548 | 14.68±0.01 | 329±3 | −11±3 |
| Q2332–094 | 3.32 | 3.05725 | 20.50±0.07 | −1.33±0.08 | S | 111 | 1550 | >14.54 | <150 | −11±6 |
| Q2343+125 | 2.51 | 2.43127 | 20.40±0.07 | −0.87±0.07 | Zn | 289 | 1550 | 14.69±0.01 | 315±3 | −137±3 |
| Q2344+125 | 2.76 | 2.53786 | 20.50±0.10 | −1.81±0.10 | Si | 69 | 1548 | 13.02±0.02 | 40±3 | −12±3 |
| Q2348–011 | 3.01 | 2.42630 | 20.50±0.10 | −0.62±0.10 | S | 248 | 1550 | >14.77 | <277 | 15±6 |
| Q2348–011 | 3.01 | 2.61473 | 21.30±0.08 | −2.02±0.08 | Si | 100 | 1548 | 13.53±0.01 | 296±4 | 11±3 |
| Q2359–022 | 2.81 | 2.09508 | 20.65±0.10 | −0.84±0.13 | Zn | 146 | 1550 | >14.87 | <131 | −92±66 |
| Q2359–022 | 2.81 | 2.15390 | 20.30±0.10 | −1.62±0.10 | Si | 67 | 1550 | >15.01 | <367 | 48±42 |

¹ The absorber redshift is defined by the velocity of the strongest component seen in the low-ionization lines.

² Taken from Ledoux et al. (2006), Smette et al. (2005), Smette et al. (2007, in preparation), Akerman et al. (2005), Ellison & Lopez (2001), or this paper. The element Z is Zn if Zn II is detected, otherwise Si or S.

³ Neutral line velocity width containing central 90% of the apparent optical depth, in km s^{-1} . The measurement is made on an optically thin line, i.e. one with $0.1 < F(v_0)/F_c(v_0) < 0.6$ (see Ledoux et al. 2006). Typical error is $\approx 3 \text{ km s}^{-1}$.

⁴ Line used to measure C IV. $\lambda 1548$ is chosen if $F(v_0)/F_c(v_0) > 0.1$, $\lambda 1550$ otherwise.

⁵ C IV column density measured using the apparent optical depth method. $N_{\text{C IV}}$ is in cm^{-2} . Lower limits are 3σ .

⁶ C IV line width containing central 90% of apparent optical depth, in km s^{-1} . Upper limits represent saturated cases.

⁷ Mean velocity of C IV absorption profile, i.e. velocity offset from neutral gas, in km s^{-1} . Errors have been doubled for saturated cases.

⁸ Both lines partly blended; results from combining measurements of absorption in two unblended velocity ranges.

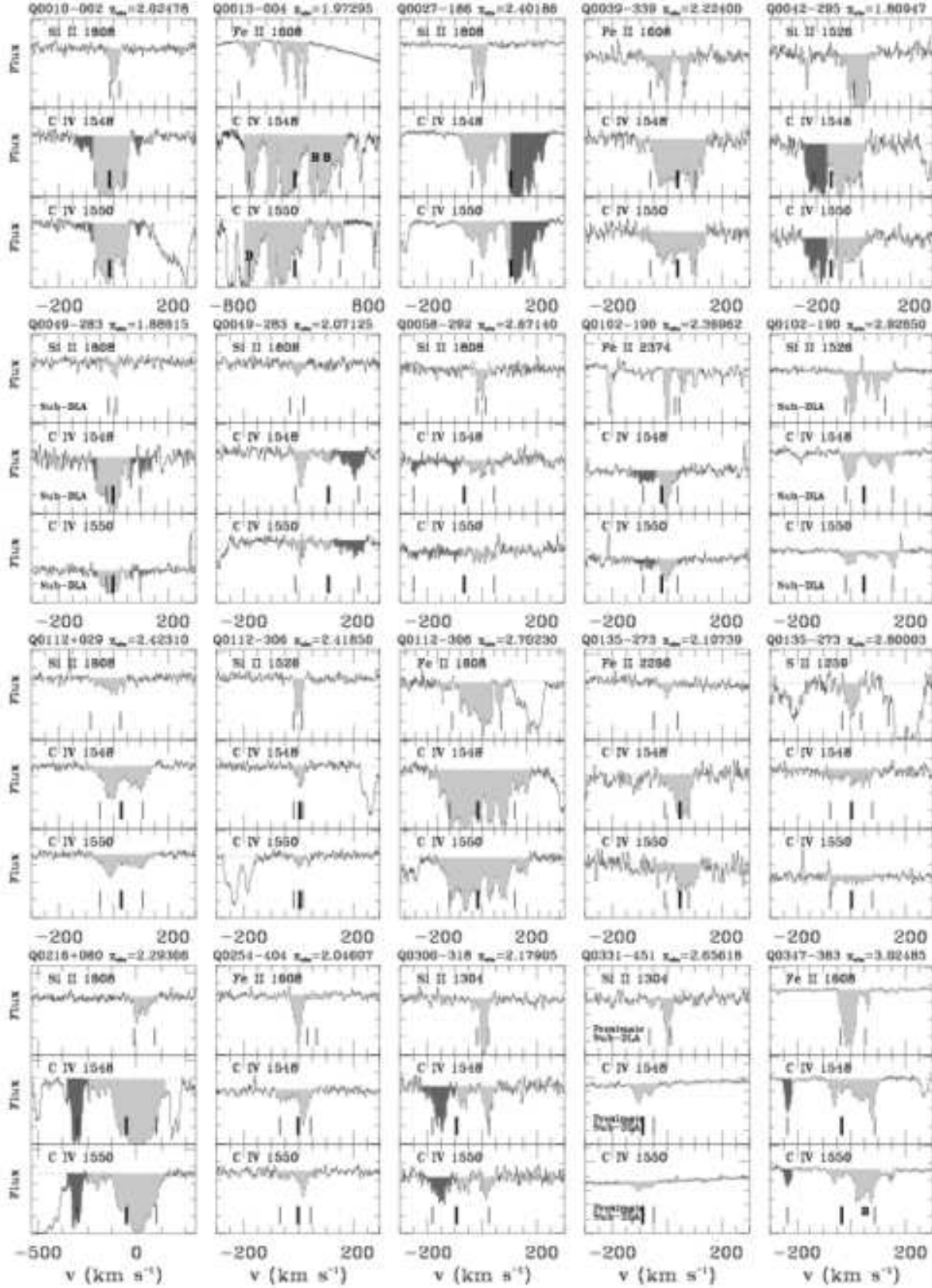


Fig. 1. VLT/UVES absorption line spectra of C IV $\lambda\lambda 1548, 1550$ and an optically thin line (typically Si II or Fe II) chosen to trace the neutral phase component structure, for all DLAs and sub-DLAs in our sample. The flux is in arbitrary units, with the bottom of each panel at zero. The light (dark) shaded regions show C IV absorption below (above) $v_{\text{esc}} = 2.4\Delta v_{\text{Neut}}$ (see text). The thick vertical line in each C IV panel denotes the optical-depth weighted mean velocity of the profile. The two narrow vertical lines show the velocities corresponding to 5% and 95% of the integrated optical depth; the interval between these velocities defines the total line width Δv . A small letter “B” within the shaded area indicates a blend; in these cases the other C IV line was used for measurement. The label “Proximate” implies the absorber is at $< 5000 \text{ km s}^{-1}$ from the QSO. Note how the wind candidate absorbers (the dark regions) show no absorption in the weak

Table 3. DLAs vs sub-DLAs, and intervening vs proximate systems

| Category ^a | # | $\langle \log N_{\text{C IV}} \rangle$ (N in cm^{-2}) | $\langle \Delta v_{\text{C IV}} \rangle$ (km s^{-1}) | $\langle \bar{v}_{\text{C IV}} \rangle$ (km s^{-1}) | $\langle \log N_{\text{H II}} \rangle$ (N in cm^{-2}) |
|------------------------|----|---|--|---|---|
| DLAs | 63 | 14.27 \pm 0.57 | 251 \pm 211 | 68 \pm 83 | 19.77 \pm 0.44 |
| Sub-DLAs | 11 | 14.07 \pm 0.67 | 272 \pm 281 | 73 \pm 54 | 19.33 \pm 0.48 |
| Intervening | 67 | 14.28 \pm 0.58 | 264 \pm 226 | 71 \pm 81 | 19.73 \pm 0.47 |
| Proximate ^b | 7 | 13.93 \pm 0.57 | 153 \pm 131 | 43 \pm 58 | 19.48 \pm 0.38 |

^a Each entry in this table shows the mean and standard deviation of the given property in the given category.^b Proximate absorbers are those within 5 000 km s^{-1} of the QSO redshift. All others are intervening

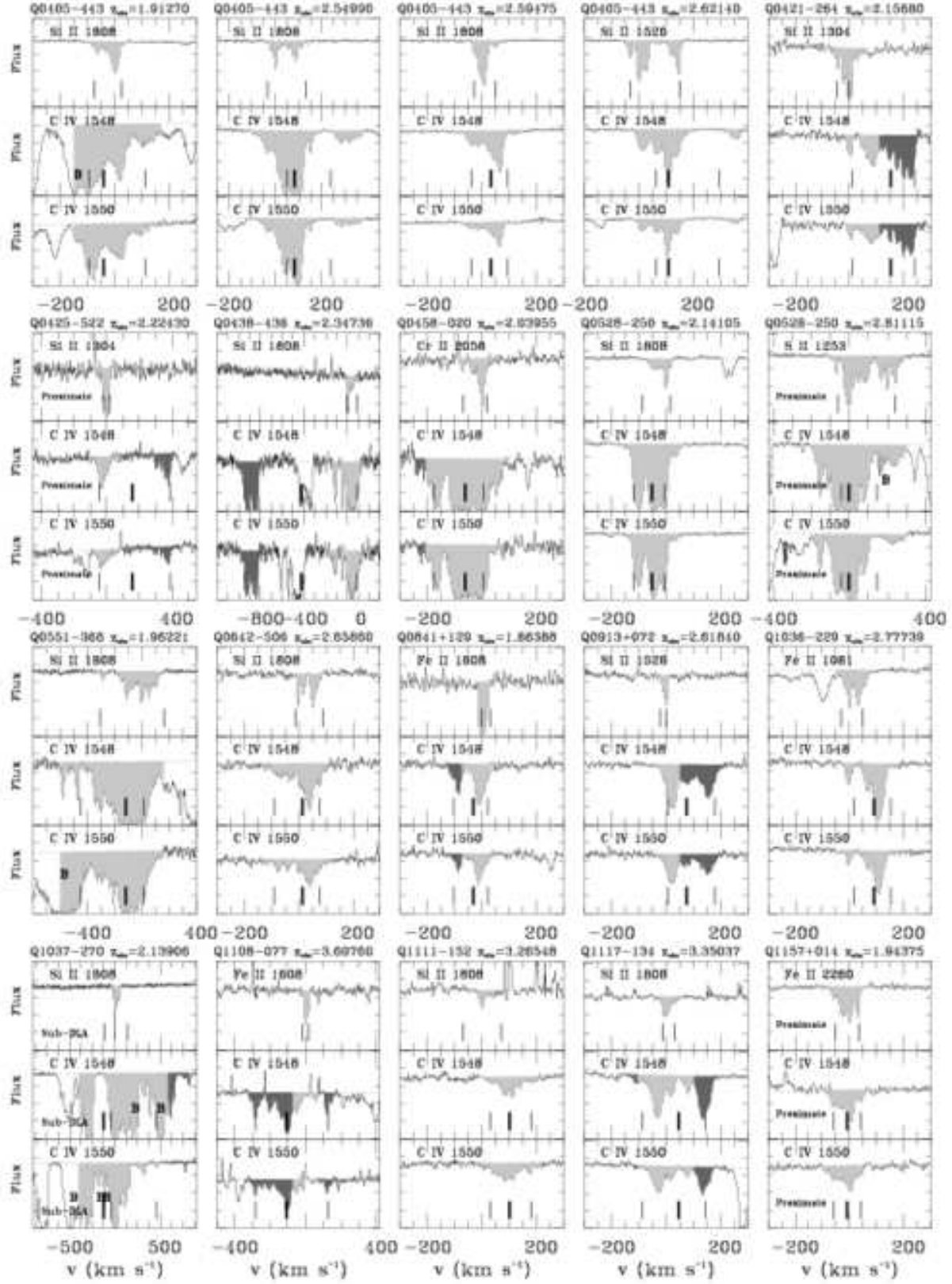


Fig. 1. (-continued).

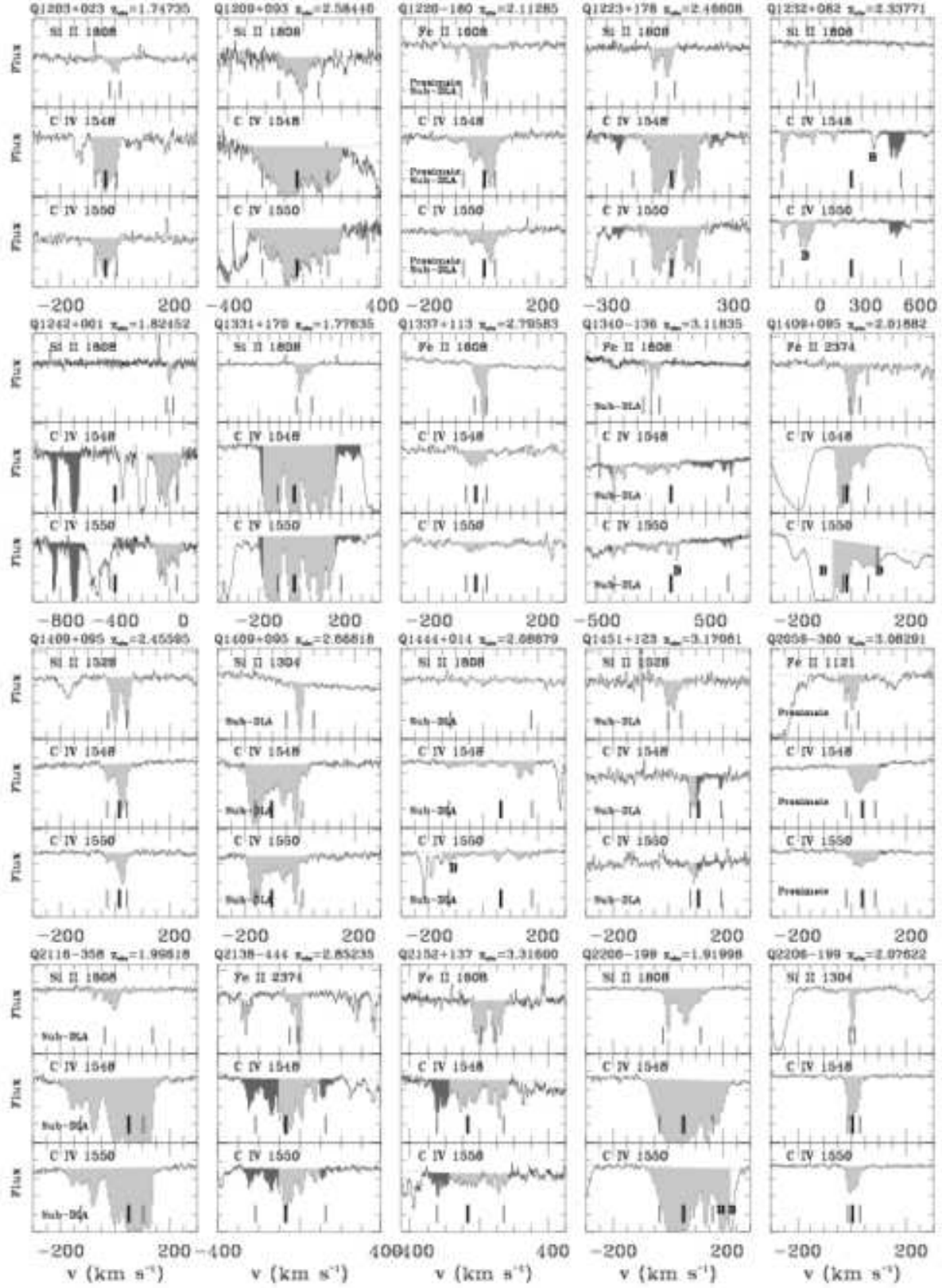


Fig. 1. (-continued).

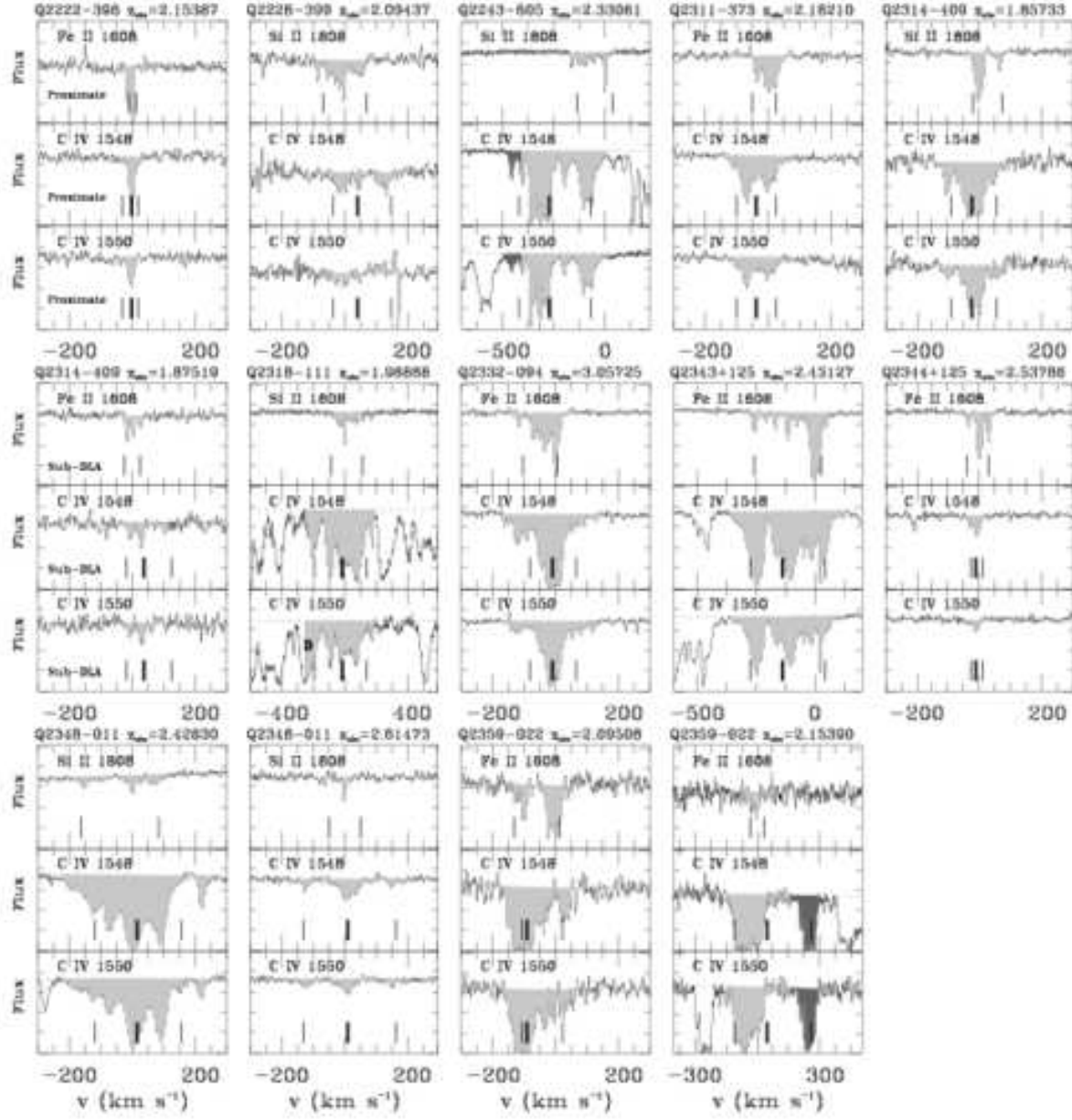


Fig. 1. (-continued).